https://doi.org/10.5194/bg-2020-69
Preprint. Discussion started: 9 March 2020

Biogeosciences Discussions

Decoupling silicate weathering from primary productivity – how ecosystems regulate nutrient uptake along a climate and vegetation gradient

Ralf A. Oeser[1], Friedhelm von Blanckenburg[1,2]

[1] GFZ German Research Centre for Geosciences, Section 3.3 Earth Surface Geochemistry, Potsdam, D-14473, Germany
[2] Freie Universität Berlin; Institute of Geological Science, Berlin, D-12249, Germany

Correspondence to: Ralf A. Oeser (oeser@gfz-potsdam.de)

Abstract. In addition to the supply of primary minerals and water flow the presence and growth rate of land plants are thought to drive rock weathering. While doubtlessly plants and their associated below-ground microbiota possess the tools for considerable weathering work, the quantitative evaluation of their impact relative to the common abiogenic weathering processes remains poorly known. Here we report on a strategy to decipher the relative impact of these two drivers. We did so by quantifying weathering rates and nutrient uptake along the "EarthShape" transect in the Chilean Coastal Cordillera where landscapes are subjected to a substantial north to south gradient in precipitation and vegetation growth, whereas rock type is granitoid throughout and tectonic process rates do not differ much along the gradient. We quantified the bio-available fraction of nutritive elements in regolith and we measured $^{87}Sr/^{86}Sr$ isotope ratios in the different compartments of the Earth's Critical Zone (bedrock, regolith, bio-available fraction in saprolite and soil, and vegetation) to identify the sources of mineral nutrients to plants. We thereby budgeted inventories, gains, and losses of nutritive elements in and out of these ecosystems, and quantified mineral nutrient recycling. We found that the weathering rates do not increase with precipitation from north to south along the climate gradient. Instead, the simultaneous increase in biomass growth rate is accommodated by faster nutrient recycling. The absence of an increase in weathering rate in spite of a five-fold increase in precipitation leads us to hypothesize that the presence of plants can negatively impact weathering through inducing secondary-mineral formation and by fostering a microbial community that is adapted for nutrient-recycling rather than nutrient-acquisition through weathering.

1 Introduction

Ever since the emergence of land plants, their dependence on mineral-derived nutrients has impacted rock weathering. This impact results from mechanical weakening of rock through roots and microbial symbionts (e.g. mycorrhizal fungi; Blum et al., 2002; Brantley et al., 2017; Hasenmueller et al., 2017; Minyard et al., 2012; Quirk et al., 2014; van Schöll et al., 2007), and from a variety of biogeochemical processes that alter the weatherability of minerals. These mechanisms include root respiration releasing protons and CO_2 which lowers the soil pH, exudation of organic ligands through roots hence increasing the solubility of nutrients by complexation, and the uptake, uplift, and recycling of pore fluids and nutrients from solution (e.g. Berner et al.,

https://doi.org/10.5194/bg-2020-69
Preprint. Discussion started: 9 March 2020


Biogeosciences Discussions Open Access EGU

2003; Brantley et al., 2012; Drever, 1994; Kump et al., 2000; Lee and Boyce, 2010; Jobbágy, 2001; Giehl and von Wiren, 2014). A third interaction affects the water cycle. The subsurface water cycle is impacted by rooting depth and seasonal water storage in saprolite, whereas the surface water cycle is affected by evapotranspiration (Kleidon et al., 2000; Ibarra et al., 2019). Because all of these interactions either directly impact weathering by aiding to acquire mineral nutrients from rock or indirectly affect weathering by modifying the water cycle (e.g. Brantley et al., 2011; Porder, 2019; Moulton et al., 2000), the presence and growth rate of land plants is commonly thought to have strongly impacted the evolution of Earth's atmosphere over geologic time by providing a negative feedback on atmospheric CO_2 concentrations (Beerling and Berner, 2005; Doughty et al., 2014; Lenton et al., 2012; Pagani et al., 2009; Porada et al., 2016).

While plants are undoubtedly key players in weathering and pedogenesis, the quantitative evaluation of their impact in these processes is a topic still widely open. The reason for this is our inability to disentangle abiotic from biotic processes during field observations (Amundson et al., 2007). Almost all mass transfer taking place in the weathering zone can have biotic and abiotic causes. Thus, field studies rely on exploring ecosystem functioning and weathering along natural environmental gradients. Studies along a Hawaiian chronosequence (soils of variable discrete initial formation age) evaluated the role of soil age on weathering and the distribution and cycling of mobile cations through plants, and discovered a strong dependency of such nutrient cycling on the degree of weathering (e.g. Bullen and Chadwick, 2016; Chadwick et al., 1999; Laliberte et al., 2013; Porder and Chadwick, 2009; Vitousek, 2004). Studies along a climosequence (gradients in climate whilst minimizing other environmental differences) evaluated the effects of climate on combined ecological and pedogenic processes (Bullen and Chadwick, 2016; Calmels et al., 2014; Dere et al., 2013; Egli et al., 2003; Ferrier et al., 2012). These studies generally show an increase in weathering rate with increasing mean annual temperature (MAT) and mean annual precipitation (MAP), while vegetation plays a significant role in pedogenesis. Studies along a lithogradient (gradients in rock substrate) evaluated the availability of nutrients and the dissolution kinetics of minerals for nutrients budgets (Hahm et al., 2014; Uhlig and von Blanckenburg, 2019) and indicate a bottom-up lithologic and mineralogic control on nutrient availability to ecosystems. Studies along gradients in erosion rates explored the supply of minerals to ecosystems and discovered an increase in nutrient supply through weathering with erosion rates (Chadwick and Asner, 2016; Eger et al., 2018; Schuessler et al., 2018). A challenge faced in many such field-based studies are the confounding effects, as environmental state variables and ecosystem properties often shift simultaneously along the gradient.

Another reason for our inability to directly attribute weathering to plant growth arises from ecosystems' ability to recycle (i.e. nutrient re-utilization through microbial mineralization from plant litter and organic matter), rather than acquiring fresh nutrients (Chaudhuri et al., 2007; Lang et al., 2016; Lucas, 2001; Spohn and Sierra, 2018; Wilcke et al., 2002). Given this ability to buffer changes in nutrient fluxes (Spohn and Sierra, 2018) the dependence of weathering on plant growth and biomass distribution would be a highly non-linear one.

Previous conceptual models of the relationship between weathering and ecosystem functioning emphasized the role of erosion, and hence landscape and nutrient supply by landscape rejuvenation for ecosystem nutrition (Buendía et al., 2010; Porder et al., 2007). Another class of models accounted for the coupled weathering – recycling – uptake systems by linking the short-term,

https://doi.org/10.5194/bg-2020-69
Preprint. Discussion started: 9 March 2020

biological cycle with the long-term, largely geological and hydrological driven cycle fostering nutrient inputs to and outputs from terrestrial ecosystems (Powers et al., 2015; Vitousek et al., 1998). Such models have recently been adapted by geochemistry (Uhlig and von Blanckenburg, 2019). In these, the so-called "organic nutrient cycle" comprises a set of strategies for efficient nutrient re-utilization through microbial mineralization from plant litter and organic matter and entails rapid nutrient turnover. However, ecosystems in sloping landscapes permanently lose these organic-derived nutrients by plant-litter erosion (Heartsill Scalley et al., 2012; Scatena and Lugo, 1995) as well as litter and root decomposition and their subsequent export in solution (Baskaran et al., 2017; Chaudhuri et al., 2007; Moore et al., 2005; Silver and Miya, 2001). Atmospheric wet and dry deposition serves as a potential replacement in tropical (e.g. Boy and Wilcke, 2008; Chadwick et al., 1999; Dosseto et al., 2012), and desert (Wang et al., 2014) ecosystems which are subject to slow erosion rates and high atmospheric input. However, in most sloping landscapes, the dominant nutrient-replacing mechanism is provided by the "geogenic nutrient pathway" which counterbalances losses by a slow but steady release of nutrients through chemical weathering of rock (Buendía et al., 2010; Cleveland et al., 2013; Uhlig and von Blanckenburg, 2019). Even though these geogenic fluxes are minor compared to the organic nutrient cycle they sustain ecosystem nutrition over the long-term (millennial) time scales. The importance of this geogenic nutrient source to sustain ecosystem nutrition with macronutrients (e.g. Ca, K, Mg, and P) over longer time scales has recently been demonstrated by several studies across a variety of biomes (Hahm et al., 2014; Schuessler et al., 2018; Uhlig et al., 2017; Uhlig and von Blanckenburg, 2019). Uhlig and von Blanckenburg (2019) found that long-term ecosystem nutrition is ensured by the adjustment of the nutrient re-utilization loop towards higher efficiency that compensates for a lower nutrient supply from chemical weathering.

However, whether the geogenic nutrient pathway is sufficiently effective to prevent development of nutrient limitation over the millennial scale depends on the supply of fresh rock into the weathering zone, the bio-availability of the nutrients released, and whether plant roots and the associated mycorrhizal fungi can access them. Thus, any exploration of these links remains inconclusive without constraining the loci of nutrient source in regolith and its stoichiometry in comparison to plant demand.

In this study, we explored weathering, nutrient uptake, and nutrient recycling along the "EarthShape" (Oeser et al., 2018) climate and vegetation gradient in the Chilean Coastal Cordillera. The four sites range from ~26°S to ~38°S and while lithology (granitoid), tectonic uplift, and erosion rates (10 to 40 t km^{-2} yr^{-1}; Schaller et al., 2018) are broadly similar, precipitation forms a gradient from 10 mm yr^{-1} in the north to 1100 mm yr^{-1}in the south (Ministerio de Obras Públicas, 2017). Similarly, net primary productivity (NPP) increases from 30 to 520 g_C m^{-2} yr^{-1} (Werner et al., 2018). Along this gradient we quantified the degree (using chemical analyses of rock and regolith, Oeser et al., 2018) and rates (using cosmogenic ^{10}Be, Schaller et al., 2018) of weathering and nutrient uptake (using NPP and the chemical composition of the major plant species at each site). Sequential extraction on bulk regolith was used to identify the stoichiometry of the main plant-available elements in the regolith (sum of saprolite and soil) in addition to phosphorus (Brucker and Spohn, 2019). We further utilized radiogenic $^{87}Sr/^{86}Sr$ isotope ratios in bulk rock, regolith, and plant samples along with those in the bio-available fraction to identify the sources of mineral nutrients. Thus, we were able to identify gains and losses of nutritive elements in and out of these ecosystems and to

https://doi.org/10.5194/bg-2020-69
Preprint. Discussion started: 9 March 2020

quantify the efficiency of nutrient recycling. We applied the conceptual framework and parameterization of Uhlig and von Blanckenburg (2019) to place quantitative constraints onto the "organic nutrient cycle" and the "geogenic nutrient pathway". We evaluated the following questions. (1) Does weathering increase from north to south along the along the EarthShape precipitation gradient, because runoff increases while other factors like mineral supply and dissolution kinetics are similar due to the similarities in erosion rate and lithology? (2) Is the increase in net primary productivity (NPP) from north to south accommodated by additional nutrient supply from weathering? We found that neither is the case. We found that weathering rate is relatively uniform, and that instead the recycling of nutrient increases along the gradient. Ultimately, we were thus able to identify processes that sustain nutrient supply in the very different ecosystems along this unique EarthShape climate and vegetation gradient.

2 Study area and previous results

The four study sites are part of the EarthShape study area which is located along the Chilean Coastal Cordillera. Three sites are located in National Parks and one on a nature reserve, so that human impact is minimized. The single sites are located within the plutonic rocks of the Chilean Coastal Cordillera and are close to the Pacific coast (less than 80 km; Oeser et al., 2018).

The sites feature a vegetation gradient controlled by climate, ranging over 1300 km. They form a sequence from north to south covering arid (Pan de Azúcar National Park, ~26°S), semi-arid (Santa Gracia Nature Reserve, ~30°S), mediterranean (La Campana National Park, ~33°S), and humid-temperate (Nahuelbuta National Park, ~38°S) climate conditions. The mean annual precipitation (MAP) increases from 10 mm yr^{-1} in Pan de Azúcar, 89 mm yr^{-1} in Santa Gracia, 440 mm yr^{-1} in La Campana, to 1100 mm yr^{-1} in Nahuelbuta, respectively. The mean annual air temperature (MAT) ranges from 18.1°C in the northernmost site in Pan de Azúcar to 14.1°C in the southernmost site in Nahuelbuta (Fig. 1, Table 1; Ministerio de Obras Públicas, 2017).

Net primary productivity (NPP), derived from a dynamic vegetation model (LPJ-GUESS) simulating vegetation cover and composition during the Holocene (Werner et al., 2018), ranges from 30 g_C m^{-2} yr^{-1} and 150 g_C m^{-2} yr^{-1} in the arid shrubland of Pan de Azúcar and Santa Gracia, respectively, to 280 g_C m^{-2} yr^{-1} in the *sclerophyllous* woodland of La Campana, and is highest (520 g_C m^{-2} yr^{-1}) in the temperate forests of Nahuelbuta (Fig. 1, Table 1). The vegetation cover (< 5%) in Pan de Azúcar consist only of small shrubs, geophytes and annual plants (Armesto et al., 1993), which are mainly present in small ravines. The vegetation in Santa Gracia belongs to the "Interior Mediterranean desert scrub of *Heliotropium stenophyllum* and *Flourensia thurifera*" formation (Luebert and Pliscoff, 2006). Plants are affected by livestock grazing (mostly goats; Bahre, 1979), and vegetation cover is generally sparse. In La Campana the vegetation (almost 100% ground cover) is part of the "Coastal Mediterranean *sclerophyllous* forest of *Lithraea caustica* and *Cryptocarya alba*" formation (Luebert and Pliscoff, 2006). The dominant vegetation in Nahuelbuta is associated with the "Coastal temperate forest of *Araucaria araucana*"

https://doi.org/10.5194/bg-2020-69
Preprint. Discussion started: 9 March 2020


Biogeosciences Discussions

formation (Luebert and Pliscoff, 2006) and covers 100% of ground area. Ecosystems at all sites are primarily nitrogen-limited (Stock et al., 2019).

The basement at those sites is mainly composed of granitoid intrusions of Cretaceous to late Carboniferous age. The compositional variation ranges from monzo- to syenogranites in Pan de Azúcar (199 Ma; Berg and Breitkreuz, 1983; Berg and Baumann, 1985; Parada et al., 2007), pyroxene and hornblende-bearing diorites and monzodiorites in Santa Gracia (98 – 89 Ma; Moscoso et al., 1982), as well as tonalites and granodiorites in Nahuelbuta (Nahuelbuta complex, 294 Ma; Parada et al., 2007) and in the Caleu Pluton in La Campana with an intrusion age of 130 Myr (Molina et al., 2015; Parada and Larrondo, 1999; Parada et al., 2002).

Catchment-wide denudation rates inferred from cosmogenic nuclides (*in situ* ^{10}Be) are lowest in Pan de Azúcar (7.7 ± 0.7 t km^{-2} yr^{-1}) and Santa Gracia (9.2 ± 0.8 t km^{-2} yr^{-1}), highest in La Campana (200 ± 22 t km^{-2} yr^{-1}), and intermediate in Nahuelbuta (27.4 ± 2.4 t km^{-2} yr^{-1}) is lower (van Dongen et al., 2019). At the soil pit scale, Schaller et al. (2018) report a trend in total soil denudation rates, interpreted as soil production rates, from Pan de Azúcar (8 – 11 t km^{-2} yr^{-1}) to Santa Gracia (16 – 22 t km^{-2} yr^{-1}) with a peak in La Campana (54 – 69 t km^{-2} yr^{-1}) and 18 – 48 t km^{-2} yr^{-1} in Nahuelbuta. The elevated catchment-wide rates at La Campana are attributed to faster erosion processes dominating the entire catchment that is characterized by higher hill slopes than in the other areas (e.g. mean slope 23° in La Campana, 9° in Nahuelbuta; van Dongen et al., 2019). They are thus towards the lower end of global cosmogenic nuclide-derived soil production rates (Dixon et al., 2012). The relative consistency of these rates along the climate gradient are ascribed to uniform tectonic forces acting in the whole study area (e.g. Blanco-Chao et al., 2014; Melnik, 2016).

The architecture of the regolith profiles, their chemistry, mineralogy, and the physical properties of soils, saprolite, and the rocks beneath have been extensively described by Bernhard et al. (2018), Dal Bo et al. (2019), Oeser et al. (2018) and Schaller et al. (2018).

The regolith profiles in Pan de Azúcar are located between 330 and 340 m a.s.l. on steep (25 – 40°; Table 1) hill slopes. The soils on the north- and on the south-facing slope were classified by Bernhard et al. (2018) as Regosols with only shallow A and B horizons of ~20 – 30 cm thickness, lacking any kind of organic layer. In this area, the processes disintegrating rock and developing regolith are mainly physical weathering attributed to a combination of insolation- and salt weathering (Oeser et al., 2018). The regolith profiles in Santa Gracia are situated at almost 700 m a.s.l. on mild sloping hills (15 – 25°; Table 1). The soils on the north- and on the soul-facing slope are a Leptosol and a Cambisol, respectively (Bernhard et al., 2018). Distinct O-horizons are not apparent. The Ah horizons in both profiles reach depths of 10 cm and the transition from the mineral soil (Bw) into saprolite occurs at 25 – 30 cm depth. Oeser et al. (2018) attribute this study sites' high degree of elemental depletion (i.e. τ, almost 60% loss of Ca and Na relative to bedrock; Fig. A1; Table S2) despite low precipitation to the low abundance of quartz and the high abundance of readily weatherable plagioclase and mafic minerals. The regolith profiles in La Campana, located at 730 m a.s.l. and on mild sloping hills (12 – 23°), are classified as Cambisols. The O-horizon is ~5 cm thick and is followed by a Ah horizon, extending up to 40 cm depth (Bernhard et al., 2018). Here, the mineral-soil layer turns into saprolite at approximately 110 cm in both profiles (Table 1). The elemental depletion of for example Ca increases accordingly from

https://doi.org/10.5194/bg-2020-69
Preprint. Discussion started: 9 March 2020

~45% at the profiles' bottom towards ~70% at their top and can be classified as depletion (north-facing) or depletion and enrichment profiles (south-facing, Fig. A1; Table S2; Brantley and Lebedeva, 2011), respectively. The regolith in Nahuelbuta are situated on gently sloping hills (~15°) at about 1200 m a.s.l. (Table 1). Bernhard et al. (2018) have classified the soils on the north- and south-facing slope as umbric Podsol and orthodystric Umbrisol, respectively. Here, the Ah horizons measure up to 50 cm (greater thickness on the south-facing slope) and are overlain by an organic horizon of 5.5 cm thickness. In the two regolith profiles, the soil-saprolite transition is at 100 and 120 cm depth, respectively. The coarse-grained saprolite disaggregates readily. These profiles are characterized by highly heterogeneous weathering patterns caused by the incorporation of the metamorphic basement at various parts (e.g. Oeser et al., 2018; Hervé, 1977).

A comprehensive summary of the eight regolith profiles' characteristics and major plant types is given in Table 1.

3 Methods

3.1 Sampling

Regolith samples were collected in a continuous sequence of depth increments from bottom to top. Increments amount to a thickness of 5 cm for the uppermost two samples, 10 cm for the 3rd sample from top, and increase to 20 cm thickness for the 4th sample onwards. To account for the dependence on solar radiation, two regolith profiles on adjacent hillslopes (north- and south-facing) were sampled at each study site.

The underlying unweathered bedrock has not been reached in either of the regolith profiles and the depth to bedrock remains unknown. Thus, bedrock samples were collected from nearby outcrops. This sample set comprises the 20 bedrock samples already reported in Oeser et al. (2018) and 15 additional bedrock samples (in total 12 in Pan de Azúcar, 8 in Santa Gracia, 10 in La Campana, and 5 in Nahuelbuta) from within the respective study sites.

Vegetation samples from representative shrubs and trees of each study site have been sampled. The sample set comprises stem-, twig-, and leaf-samples from mature plants of the prevailing species *Nolana mollis* (Pan de Azúcar), *Asterasia* sp., *Cordia decandra*, *Cumulopuntia sphaerica*, and *Proustia cuneifolia* (Santa Gracia), *Aristeguietia salvia*, *Colliguaja odorifera*, *Cryptocarya alba*, and *Lithraea caustica* (La Campana), *Araucaria araucana*, *Nothofagus antarctica*, and *Chusquea coleu* (Nahuelbuta), respectively. These samples were either taken using an increment borer (stem samples) or plant scissors (leaf and twig samples) equipped with a telescopic arm to reach the higher parts of trees. In addition, the litter layer in La Campana and Nahuelbuta was sampled.

3.2 Analytical methods

3.2.1 Chemical composition of regolith and bedrock

The concentration of major and trace elements in bedrock and regolith samples were determined using a X-Ray Fluorescence spectrometer (PANalytical AXIOS Advanced) at the section for "Inorganic and Isotope Geochemistry", GFZ German

https://doi.org/10.5194/bg-2020-69
Preprint. Discussion started: 9 March 2020

Research Centre for Geosciences. A detailed description of the analytical protocols and sample preparation is given in Oeser et al. (2018).

3.2.2 Chemical composition of vegetation

Major and trace element concentrations of vegetation samples were determined using a Varian 720-ES axial ICP-OES at the Helmholtz Laboratory for the Geochemistry of the Earth Surface (HELGES), GFZ German Research Centre for Geosciences (von Blanckenburg et al., 2016) with relative uncertainties smaller than 10%. Prior to analysis, all samples were oven-dried at 120°C for 12 hrs. Subsequently, leaves were crushed and homogenized. About 0.5 g of leaf and 1 g of woody samples were digested in PFA vials using a microwave (MLS start) and ultra-pure concentrated acid mixtures comprising H_2O_2 and HNO_3, HCl and HNO_3, and HF. In some plant samples Si-bearing precipitates formed upon evaporation after digestion. These sample cakes were redissoled in a mixture of concentrated HF and HNO_3 to ensure complete dissolution of Si prior to analysis. As some Si might have been lost by evaporation in this process, we have not included these plant samples (indicated by a * in Table S5) for the compilation of the plants' Si budget. With each sample batch, the international reference material NIST SRM 1515 Apple leaves and a procedural blank was processed.

3.2.3 Extraction of the bio-available fraction and its chemical analyses

The bio-available fraction of regolith samples was extracted using a sequential extraction procedure adapted from Arunachalam et al. (1996), He et al. (1995), and Tessier et al. (1979). The sequential extraction was performed in parallel on two regolith aliquots, of which the supernatants were pooled together for analyses. About 2 g of dried and sieved (<2 mm) sample material were immersed in 14 ml either 18 MΩ Milli-Q H_2O (water-soluble fraction) or in 1M NH_4Oac (exchangeable fraction), thus maintaining a sample to reactant ratio of about 1:7. Each extraction step was performed with mild agitation. After each extraction, the mixture was centrifuged for 30 min at 4200 rpm and the supernatant was pipetted off. The remaining sample was then rinsed with 10 ml Milli-Q H_2O and centrifuged again (4200 rpm, 30 min). This rinse solution was added to the supernatant. Subsequently, the supernatants were purified using a vacuum-driven filtration system (Millipore®; 0.2 µm acetate filter), evaporated to dryness, and redissolved with ultra-pure concentrated acid mixtures comprising H_2O_2, HNO_3, and HCl. With each sample batch, international reference materials (NIST SRM 2709a San Joaquin soil, CCRMP TILL-1) along with a procedural blank were processed.

The water-soluble fraction is comprised of elements contained in soil water in the form of free ions and ions which form complexes with soluble organic matter. It represents the most labile soil compartment and thus is most accessible to plants (e.g. He et al., 1995). This fraction was accessed by suspending the samples for 24 hrs in Milli-Q H_2O at room temperature. The exchangeable fraction constitutes of elements that form weak electrostatic bonds between the hydrated surfaces of phyllosilicates (i.e. clays and micas), oxyhydroxide minerals (e.g. boehmite, diaspore, goethite, lepidocrocite, ferrihydrite), and organic matter. This fraction was extracted by suspending the samples in a mechanical end over end shaker at room temperature in 1 M NH_4OAc for 2 hrs at 60 rpm. Note that none of the further extraction steps described in Tessier et al. (1979)

https://doi.org/10.5194/bg-2020-69
Preprint. Discussion started: 9 March 2020

has been applied to the regolith samples in this study as they are believed to make a negligible contribution to the bio-available fraction.

The element concentrations of the water-soluble and exchangeable fraction were determined using a Varian 720-ES axial ICP-OES at HELGES, following the analytical procedures described in Schuessler et al. (2016) with relative uncertainties estimated at smaller than 10%.

The soil-P fractions were determined by Brucker and Spohn (2019). In this case, the bio-available fraction refers to the inorganic products of the modified Hedley sequential P fractionation method of Tiessen and Moir (1993), specifically the water-extractable P_i and labile P_i which was extracted by using 0.5 M $NaHCO_3$.

3.2.4 $^{87}Sr/^{86}Sr$ isotope ratios

The radiogenic Sr isotope ratio was determined on bulk bedrock and regolith, the bio-available fractions of saprolite and soil, and on the different plant organs at each study site.

Upon sample digestion (bulk samples) or sequential extraction (bio-available fraction), Sr was separated from matrix elements using 200 µl Sr-Spec resin. Matrix elements were removed by elution with 2.5 ml 3 M and 2 ml 7.5 M HNO_3. Subsequently, Sr was eluted with 4 ml of 18 Ω Milli-Q H_2O. Any organic crown-ether which has been released from the Sr-spec resin was removed after evaporation and subsequent redissolution of the Sr fraction in 1 ml of a 1:1 mixture of concentrated H_2O_2 and HNO_3. This mixture was cooked in a tightly closed beaker at 150°C for at least 12 hrs. Within each sample batch, a minimum of one standard reference material and a procedural blank were processed.

$^{87}Sr/^{86}Sr$ was measured in a 50-ng g^{-1} pure Sr solution in 0.3 M HNO_3 using a multi collector inductively coupled plasma mass spectrometer (MC-ICP-MS, Thermo Neptune) in medium mass resolution. The MC-ICP-MS was equipped with an APEX-Q (ESI) desolvating nebulizer with uptake rates of 70 µl min^{-1} and a nickel sampler cone. Radiogenic Sr isotope ratios were determined over one block of 20 cycles with an integration time of 16 seconds each. The sequence of a sample run was comprised of 10 to 12 blocks, where each block comprised a blank, four samples, and five SRM 987 which were not processed through chemistry. Blank correction of samples and reference material during the sequence was less than 0.4% of the sample signal. The intensities of the ion beams on the masses ^{82}Kr (L4), ^{83}Kr (L3), ^{84}Sr (L2), ^{85}Rb (L1), ^{86}Sr (central Faraday Cup), ^{87}Sr (H1) and ^{88}Sr (H2) were monitored using Faraday collectors equipped with 10^{11} Ω resistors. Isobaric interference on the masses 84, 86, and 87 were corrected for with the Kr and Rb isotope ratios measured prior to the sequence run. To correct for any natural and instrumental isotope fractionation, the measured $^{87}Sr/^{86}Sr$ ratio was normalized to the $^{88}Sr/^{86}Sr$ ratio of 8.375209 (Nier, 1938's value) by using an exponential law. Finally, the $^{87}Sr/^{86}Sr$ ratios were corrected for a session offset.

3.3 Parameterizing geogenic and biogenic element fluxes in a terrestrial ecosystem

The parameterization of the “geogenic nutrient pathway” and the “organic nutrient cycle” (Fig. 2) to characterize element fluxes into, within, and from the Critical Zone and its ecosystem components, including the derivation of the corresponding equations has been thoroughly described in Uhlig and von Blanckenburg (2019). Because throughout this article we make use

https://doi.org/10.5194/bg-2020-69
Preprint. Discussion started: 9 March 2020

of this framework we only briefly summarize the metrics, which are shown in Table 2. Calculation and parameters used for these metrics are presented Appendix A.

4 Results

We structure the presentation of our results in the following sequence: (1) the element fluxes of the geogenic nutrient pathway; (2) the availability of elements in regolith to plants; and (3) the plants' chemical composition along with the element fluxes that link the geogenic nutrient pathway to the organic nutrient cycle.

We focus the detailed presentation of these results on the two most important mineral nutrients to plants P and K, and further provide data on the plant-essential elements Ca, K, Mg, and Mn as well as plant-beneficial elements Al, Fe, Na, and Si (Marschner, 1983). In this presentation, we treat both Sr and Ca as plant-essential elements due to their similar (bio-) chemical behavior (e.g. Blum et al., 2012; Faure and Mensing, 2005; Faure and Powell, 1972; Poszwa et al., 2002).

4.1 Element fluxes contributing to the geogenic nutrient pathway

4.1.1 Degree of weathering and elemental gains and losses

The chemical depletion fraction (CDF; Table 2, Eq. 5) and elemental mass transfer coefficient (τ; Table 2, Eq. 6) disclose the total and the element-specific loss, respectively, of soluble elements relative to bedrock. Thus, both metrics quantify the degree of weathering. The average CDF of the shallowest mineral soil (combined analysis of north- and south-facing profiles) in Pan de Azúcar, Santa Gracia, La Campana, and Nahuelbuta amounts to 0.03, 0.54, 0.50, and 0.25, respectively (Fig. 3; Table S2). At all four sites, the elemental losses (Fig. A1; Table S2) can be attributed to a "kinetically limited weathering regime" (Brantley and Lebedeva, 2011). This means that the erosion rate is at a sufficient level to continuously replenish the nutrient stock held in weatherable minerals that transit vertically through the weathering profile.

Systematic differences in chemical depletion pattern (i.e. CDF and τ) that arose from different combinations of (micro-) climate and biota between north- and south-facing slopes are not discernible or, as is the case of La Campana, caused by anomalous high Zr concentrations throughout the entire north-facing profile. Moreover, we found that neither CDF nor τ systematically differ between Santa Gracia, La Campana, and Nahuelbuta.

A comprehensive presentation of these data can be found as Appendix in Fig. A1 and in the supplementary Table S2 (Oeser and von Blanckenburg, 2020).

4.1.2 Elemental chemical weathering fluxes

$W^{X}_{regolith}$ (Table 2, Eq. 3) quantifies the elemental release fluxes from rock and regolith by weathering and thus the weathering supply of nutrients to ecosystems. The weathering release for the most plant-essential rock-derived mineral nutrient phosphorus $W^{P}_{regolith}$ in Pan de Azúcar, Santa Gracia, La Campana, and Nahuelbuta amounts to 1.3, 12, 19, and 11 mg m^{-2} yr^{-1},

https://doi.org/10.5194/bg-2020-69
Preprint. Discussion started: 9 March 2020

respectively, and those of the similarly plant-essential element potassium ($W^{K}_{regolith}$) to 30, 80, 840, and 100 mg m^{-2} yr^{-1} (Fig. 4, Table 3). $W^{X}_{regolith}$ of the plant-beneficial elements Al, Na, and Si along with Fe and Sr follow the trend described for K and P. The weathering supply fluxes of both P and K as well as the plant-beneficial elements in Santa Gracia and Nahuelbuta are thus in a similar range despite severe differences in MAP, NPP, and vegetation cover. $W^{Ca}_{regolith}$ and $W^{Mg}_{regolith}$ do deviate from this general pattern such that these elements' highest weathering-release fluxes are attained in Santa Gracia followed by La Campana, Nahuelbuta, and Pan de Azúcar. These elevated weathering release fluxes of Ca and Mg in Santa Gracia are attributed to the bedrocks' initial mineralogy, and their high Ca and Mg concentration (Table S1).

4.2 Availability of mineral nutrients to ecosystems

The maximum amount of nutrients present can be assessed by determining their inventory in bulk regolith (I^{X}_{bulk}; Table 2, Eq. 8). For most elements, apart from K and Si, the inventory of potentially available elements is by far greatest in Santa Gracia (Table 4). I^{X}_{bulk} in the other three study sites are mostly at a similar level. Note that only a minor fraction of this bulk nutrient inventory is readily bio-available.

The element concentration in the bio-available fraction are some orders of magnitude below the concentrations in bulk regolith (Fig. A2 & A3, Table S3). Bio-available P in saprolite ($I^{P}_{bio\text{-}av,\ sap}$) is virtually absent in Pan de Azúcar and amounts to 21, 39, and 23 g m^{-2} in Santa Gracia, La Campana, and Nahuelbuta, respectively (Table 4). $I^{K}_{bio\text{-}av,\ sap}$ equals 253 in the northernmost, and 23, 70, and 19 g m^{-2} in the other study sites further south, respectively. Bio-availability of the remaining mineral nutrients in saprolite is high in Santa Gracia and La Campana, and low in Pan de Azúcar and Nahuelbuta (Table 4). Note that $I^{K}_{bio\text{-}av,\ sap}$ was calculated over the uppermost 1 m of saprolite, whereas in fact the zone of mineral nutrient extraction might extend deeper.

Bio-availability of most elements in soil, bar a few exceptions, increase from Pan de Azúcar to La Campana. However, despite featuring the thickest soils, bio-availability is lowest in Nahuelbuta. Exceptions from this general trend are P and K. $I^{P}_{bio\text{-}av,\ soil}$ amounts to 3.3 g m^{-2} in Pan de Azúcar and 22 g m^{-2} in Santa Gracia and is as high as 28 and 31 g m^{-2} in La Campana and Nahuelbuta, respectively (Table 4). $I^{K}_{bio\text{-}av,\ soil}$ amounts to 53, 38, 90, and 38 g m^{-2} in Pan de Azúcar, Santa Gracia, La Campana, and Nahuelbuta, respectively. Thus, K is almost equally available to plants in the four study sites.

4.3 Plant element composition and nutrient-uptake fluxes

Average elemental concentrations in bulk plants decrease from Pan de Azúcar towards Nahuelbuta. The exception is P, whose average concentration increases from 290 µg g^{-1} in Pan de Azúcar to 1400 µg g^{-1} in Nahuelbuta (Table 5). The average K concentration amounts to 6900, 6400, 12000, and 5400 µg g^{-1} along the EarthShape climate and vegetation gradient from north to south. Thus, in Pan de Azúcar, Santa Gracia, and Nahuelbuta, average K concentrations are in a similar range, whereas in La Campana, K concentration in plants is almost twice as high compared to the other three sites.

https://doi.org/10.5194/bg-2020-69
Preprint. Discussion started: 9 March 2020

The nutrient-uptake fluxes of the two most important rock-derived mineral nutrients to plants, P and K, increase steadily from north to south, such that U^{P}_{total} amounts to 5, 70, 170, and 350 mg m^{-2} yr^{-1} and U^{K}_{total} to 110, 500, 2000, and 1400 mg m^{-2} yr^{-1} in Pan de Azúcar, Santa Gracia, La Campana, and Nahuelbuta, respectively (Table 3).

U^{X}_{total} of the plant-essential elements Ca, K, Mg, Mn, P, and Sr exceed $W^{X}_{regolith}$ up to several times. U^{X}_{total} and $W^{X}_{regolith}$ are close to identical for Mg, Mn, and Sr in La Campana (Fig. 4; Table 3). U^{X}_{total} of the remaining plant-beneficial elements are, apart from Fe and Na in Pan de Azúcar, always lower than their release by weathering.

4.4 $^{87}Sr/^{86}Sr$ isotope ratios

Radiogenic Sr isotope ratios on bulk bedrock and regolith samples disclose mineral-weathering reactions and the incorporation of external sources into the regolith profiles. Moreover, $^{87}Sr/^{86}Sr$ in the bio-available fraction and plants reveal the plants' mineral nutrient sources.

In Pan de Azúcar, the $^{87}Sr/^{86}Sr$ ratio of bulk regolith ranges from 0.723 to 0.737 and is distinct from average bedrock (0.726 ± 0.002; Fig. 5, Table 6). The Sr isotope ratios differ significantly between the two regolith profiles which can be attributed to the varying degrees of atmospheric deposition ($^{87}Sr/^{86}Sr_{seaspray}$ = 0.7092; Pearce et al., 2015). $^{87}Sr/^{86}Sr$ ratios in the bio-available fraction of saprolite and soil deviate by 0.02 from those of bulk bedrock and regolith but do not vary considerably between saprolite and soil, and the north- and south-facing slopes, respectively. Bulk plant samples yield $^{87}Sr/^{86}Sr$ ratios of 0.710 and are thus indistinguishable from the $^{87}Sr/^{86}Sr$ ratio in the bio-available fraction (0.710 ± 0.001; Fig. 5, Table 6).

In Santa Gracia, the $^{87}Sr/^{86}Sr$ ratios in both bedrock and the regolith profiles do not deviate significantly from each other ($^{87}Sr/^{86}Sr_{rock}$ = 0.7039 ± 0.0004, $^{87}Sr/^{86}Sr_{regolith}$ = 0.7043 ± 0.0003; Fig. 5, Table 6). The radiogenic Sr composition of the bio-available fractions in saprolite and soil are identical within uncertainty, and no differences in $^{87}Sr/^{86}Sr$ between the north- and south-facing regolith profile are apparent. Plants yield an average $^{87}Sr/^{86}Sr$ ratio of 0.7062 ± 0.0001 and are thus indistinguishable from the bio-available fractions in saprolite and soil (Fig. 5, Table 6).

The bulk regolith $^{87}Sr/^{86}Sr$ ratio in La Campana ranges from 0.7051 in the N-facing to 0.7055 in the south-facing regolith profile. This ratio is a substantially lower than in bedrock (0.7061 ± 0.0003; Fig. 5, Table 6) which can be attributed to the loss of a mineral with a high $^{87}Sr/^{86}Sr$ isotope ratio (e.g. biotite) beneath the depth of the sampled regolith profiles. The radiogenic Sr composition of the bio-available fraction in saprolite and soil amounts to 0.7051 and 0.7053, respectively, and is within the range of bulk regolith. Here, the difference in the $^{87}Sr/^{86}Sr$ ratio between the north- and the south-facing regolith profile increases from bulk regolith to the bio-available fraction in saprolite and is highest in the soil bio-available fraction. The average $^{87}Sr/^{86}Sr$ ratio in plants is 0.7059 and can be as high as 0.7063 in *Cryptocaria alba* (Table S7) and is thus slightly higher than in the soil and saprolite bio-available fraction. All these ratios are lower than in bulk bedrock.

In Nahuelbuta the radiogenic Sr isotope ratio in bedrock (0.716 ± 0.007) is in good agreement to those reported by Hervé et al. (1976) for the granitoid basement (0.717). However, the large spread among the bedrock samples is remarkable and denotes to the high petrological and chemical variability of the Nahuelbuta mountain range (e.g. Hervé, 1977). Thus, $^{87}Sr/^{86}Sr$ in

https://doi.org/10.5194/bg-2020-69
Preprint. Discussion started: 9 March 2020

regolith is subject to a high variability as well (Fig. 5, Table 6 & S2). The $^{87}Sr/^{86}Sr$ ratios in both bio-available fractions in Nahuelbuta are restricted to a relatively narrow range in both regolith profiles, and amount to 0.711 ± 0.002 and are thus indistinguishable from the ratios in plants (Fig. 5, Table 6). Individual plants' radiogenic Sr signature are distinct from each other and reflect the slope's bio-available fraction they grow on.

5 Discussion

5.1 The source of mineral nutrients

The radiogenic Sr composition of the bio-available fractions in saprolite and soil along with those of bulk plant serves as a proxy for the plants' nutrient sources. In all four study sites, plants take up their Sr from the bio-available fraction. In the arid site Pan de Azúcar this Sr pool is formed by Sr deposition from atmospheric sources (e.g. up to 93% seaspray contribution; Table 6). In the mediterranean and humid sites of La Campana and Nahuelbuta, respectively, the bio-available Sr is supplied by release from rock and regolith through weathering. In semi-arid Santa Gracia, we found a combination of both sources (up to 43% seaspray contribution; Table 6). In La Campana we found evidence for a deep nutrient source (located between the bottom of the regolith profile and unweathered rock) in the elemental-depletion pattern (Fig. A1). Here, deep-rooting plants (e.g. *Lithraea caustica*; Canadell et al., 1996) bypass the bio-available fraction of saprolite and soil and take up Sr with a higher proportion of radiogenic ^{87}Sr which has been released through biotite weathering beneath the regolith profiles.

5.2 Are nutrient sources setting plant stoichiometry?

We expand the analysis of the source and demand of mineral nutrients, which in the preceding section was based solely on Sr as plant-essential element, to all other plant-essential (P, K, Ca, Mg, Mn) and plant-beneficial (Al, Fe, Na, Si) elements. We note that the ecosystems in the EarthShape study sites are mostly N-limited (Stock et al., 2019), yet we consider the essential mineral nutrients to be potentially co-limiting. To do so, we first evaluate whether "ecological stoichiometry" has been attained by the plants. Ecological stoichiometry suggests that, similar to ocean microbial biomass, an optimum C:N:P ratio is attained – the "Redfield ratio" (e.g. Redfield, 1934). However, it is less clear whether such stoichiometrical pattern is also valid for terrestrial ecosystems, and for other elements besides C, N, and P (Cleveland and Liptzin, 2007; Sardans et al., 2011). As pointed out by several authors (e.g. Elser et al., 2010; Geider and La Roche, 2002; Hillebrand et al., 2014; White et al., 2006), photoautotrophs only exploit a weak stoichiometric homeostasis. Hence, the elemental composition in plants (i.e. ecological stoichiometry; Sterner and Elser, 2003) is mainly set by the nutrient-supplying reservoirs ('you are what you root in model'; Elser et al., 2010), and only to a second order by homeostasis. Evidence for this suggestion was provided by Uhlig and von Blanckenburg (2019) for a large number of mineral nutrients. In that study, it was shown that the plant-available fraction in saprolite and soil is well correlated with the ecological stoichiometry in two forested ecosystems and that deviations from that trend may have been driven by demand.

https://doi.org/10.5194/bg-2020-69
Preprint. Discussion started: 9 March 2020

As an evaluation of the hypothesis that the nutrient reservoir sets plant stoichiometry we normalized both the mineral nutrient concentrations in plants (Table 5) and those in the bio-available fraction in saprolite and soil (Table S3) by the most plant-essential mineral nutrient P (Fig. 6). In this analysis, an element X that plots on the 1:1 line would fulfill the entirely hypothetical condition of being perfectly co-limited and that its relative composition is set by the relative composition in the plant-available fraction (i.e. "optimum" stoichiometric range). Such pattern would be similar to an ocean Redfield ratio in which a C:N:P ratio is identical between seawater and marine micro-biota (Capek et al., 2018; Moore et al., 2013). Elements that plot beneath the 1:1 line are available in excess in the bio-available fraction relative to P. In contrast, elements that plot above this line would be enriched in plants by their homeostasis relative to P over the X:P ratio of the bio-available fraction. Hence, this means that this element would be limiting plant growth rather than P.

Four main features characterize the ecosystems' stoichiometry along that climate transect: (1) Indeed, all elements plot close to the 1:1 line while the deviations from the line exhibit an only weak control by homeostasis. Thus, the release of elements by weathering and supply by seaspray (in Pan de Azúcar) is setting the composition of the bio-available fraction, which to a first order is setting plant stoichiometry. (2) At all sites K is taken up from the bio-available fractions in preference over P. According to the rationale of this diagram (Capek et al., 2018; Moore et al., 2013), K would be the limiting mineral nutrient rather than P, as it appears to be in higher demand than P. Evidence against this possibility are plant P concentrations that increase along the gradient, hinting at possible P limitation. This might be caused by the P fraction in the studied 1-2m of regolith shifting from the plant-available apatite fraction to less available secondary mineral P from north to south (Brucker and Spohn, 2019). In contrast, concentrations of plant-available K are rather uniform (Table S3). (3) The plant-beneficial elements (Na, Fe, Al, Si) are available in surplus only in La Campana and Nahuelbuta. Thus, at these sites a sorbed pool of these elements, which are initially released by weathering exists that is not strongly plant-utilized, whereas at the (semi-)arid sites plants make use of the full weathering release. (4) X:P ratios increasingly approach the "optimum" stoichiometric range with increasing NPP. They do this more pronounced in soil than in saprolite. So how do these gradients on stoichiometry develop together with NPP even though weathering rates are rather uniform between sites?

5.3 Nutrient recycling as buffering mechanism

The recycling of the most plant-essential mineral nutrients is the key mechanism enabling differences in NPP despite near-constant weathering rates. As seen in Figure 4 elemental uptake rates U^{X}_{total} of the most plant-essential nutrients P, K, and Ca increase in spite of rather uniform release rates from Santa Gracia to Nahuelbuta by weathering $W^{X}_{regolith}$. This recycling is quantified by the recycling factor Rec^{X} (Table 2, Eq. 7; Table 7; note that in this discussion we use the Rec^{X} calculated for $W^{X}_{regolith}$ from weathering only. In Table 7 and Fig. A4 we also show Rec^{X} including atmospheric inputs). For example, K is recycled 3 times through biomass after release by weathering at the arid site and 15 times at the humid site. P is recycled 4 times in the arid site, and 30 times in the humid site. Ca shows a similar, albeit weaker difference. Moreover, we found evidence

https://doi.org/10.5194/bg-2020-69
Preprint. Discussion started: 9 March 2020

that recycling of K through plants (Fig. 4) increases its availability in soil relative to saprolite over the entire climate gradient (Fig. 6).

Furthermore, with increasing recycling efficiency (Table 7) the nutrient pools in the bio-available fraction are increasingly dominated by the pool of recycled nutrients, thus shifting the stoichiometry in the bio-available fraction with increasing proportion of recycling successively towards the stoichiometry in vegetation (Fig. 6). In other words, over the course of several recycling loops, the chemical composition of the bio-available fraction and biota eventually approaches a ratio close to the relative requirement of the ecosystem for the different nutrients (Vitousek et al., 1998), ultimately resulting in a virtually almost perfect stoichiometric yield (Sterner and Elser, 2003). P also obtains an increasingly biocycled speciation where the total organic P fractions increase strongly along the gradient (Brucker and Spohn, 2019). In Nahuelbuta Ca, K, Mg, and Sr are taken up in excess over P. Here, organic-bound P is not as easily available, whereas the plant-availability of these elements might increase due to the higher potential for solubilization at the lower pH in soil (soil pH = 4 – 4.5; Bernhard et al., 2018). Thus, the amplitude of recycling varies from nutrient to nutrient and site to site (Table 7). In the arid Pan de Azúcar, nutrients are primarily being recycled after photodegradation of shrubs (e.g. Gallo et al., 2006; Day et al., 2015). In the remainder sites Rec^{x} increases from Santa Gracia to Nahuelbuta and is highest for the plant-essential elements Ca, K, and P (Table 7). Thus, despite having the smallest nutrient inventory of bio-available nutrients but highest NPP of these sites, the ecosystem of Nahuelbuta can at least partially maintain its nutrient requirements through efficient nutrient recycling.

Particular conditions of plant nutrition prevail at the arid sites. In Pan de Azúcar and Santa Gracia elemental concentrations in plants are exceptionally high (bar P and K; Table 5), even though these sites' nutrient-availability through weathering and water availability is generally low (Table 3 & S2). This elevated mineral-nutrient storage is typical for plants growing in infertile habitats. Through such intermediate storage, plants accumulate an internal nutrient pool that is available for homeostasis when growth conditions eventually improve during, for example, rare rain events (e.g. Chapin III, 1980; Chapin III et al., 2011; Vitousek et al., 1998). High amounts of Al and Na are being incorporated into the plants' tissues in the arid and semi-arid sites, elements that tend to be harmful and hinder plant growth when concentration is high (e.g. Delhaize and Ryan, 1995; Kronzucker and Britto, 2011). However, Al-toxicity is prevented in these plants by accumulation of similarly high amounts of Si that compensates the effects of Al (Liang et al. (2007). The Na concentrations in *N. mollis* in Pan de Azúcar are up to three orders of magnitude higher compared to the other study sites. This exceptional high Na concentration is typical of the metabolism of *N. mollis* which is known be covered with salt glands on their leaves, aiding to retrieve water by directly condensing moisture from unsaturated air (Rundel et al., 1980; Mooney et al., 1980).

5.4 How the organic and the geogenic nutrient pathway set the size of the bioavailable pool

Both our data on ecological stoichiometry and the radiogenic Sr isotopic composition suggest that the bio-available pool in saprolite and soil feeds plants. In none of our sites is the bio-available nutrient pool entirely depleted (Table 4). The concentrations of the most plant-essential and bio-available mineral nutrients K, Ca, and Mg in saprolite are highest in the arid site, lower in the semi-arid and mediterranean site, and lowest in the humid-temperate site. The element concentration in the

https://doi.org/10.5194/bg-2020-69
Preprint. Discussion started: 9 March 2020

bio-available fraction translates into the size of the inventory (note, however, that the inventory can in fact be larger than the 1 m inventory that we have used for its calculated to allow a comparison. This is suggested by the elevated $^{87}Sr/^{86}Sr$ ratios in plants at La Campana suggesting extraction of a pool beneath the bio-available upper saprolite). Regardless, given that neither these pool sizes nor the concentrations of the bio-available elements correlate with elemental release rates $W^{X}_{regolith}$, gradients in pool sizes cannot solely be explained by differences in weathering rate. Further, the differences in the pool size cannot be explained by the lack of fresh primary minerals. All four sites represent kinetically limited weathering regimes (Oeser et al., 2018) such that primary minerals are permanently available for dissolution and in turn for replenishing the bio-available pool. We thus consider next pedogenic properties as pool size-controlling factors.

The decrease of soil pH from 8 at the arid to 4 at humid site (Bernhard et al., 2018) might cause the decrease in the bio-available divalent base cations Mg, Ca, and Sr. However, the decrease in pH could in turn be the result of the loss of these elements and thus their pH buffering capacity. Another possibility are the higher concentrations of soil organic carbon (Bernhard et al., 2018) at the mediterranean and the humid sites compared to the arid sites. We regard this cause as unlikely as those elements like Al, Fe(III), and P that are readily complexed and thus lost as organic complexes are higher in the humid and mediterranean sites than the other two sites. The cation exchange capacity CEC_{eff} (Table 1; Bernhard et al., 2018) exceeds the element concentration in the bio-available fraction in the semi-arid (85 $\mu mol_C\ g^{-1}$ vs. 35 $\mu mol\ g^{-1}$), mediterranean (80 $\mu mol_C\ g^{-1}$ vs. 40 $\mu mol\ g^{-1}$), and humid-temperate (30 $\mu mol_C\ g^{-1}$ vs. 6 $\mu mol\ g^{-1}$) site. Thus, exchange sites are available in excess and do not set the maximum pool size. As a result where fluid residence times are long the bio-available fraction, formed by precipitation and sorption from pore fluids, is likely close to equilibrium with regolith fluid (Maher and Chamberlain, 2014). Only at sites with high MAP regolith fluids might be diluted and deviate from a chemostatic behavior (e.g. Godsey et al., 2019), and these fluid concentrations will be below equilibrium concentrations. No discharge data is available for the EarthShape sites, but with MAP slightly > 1000 mm yr^{-1} a dilution effect might be in effect at Nahuelbuta for elements like Mg and Ca that tend to switch from chemostatic to dilution behavior at high discharge (e.g. Godsey et al., 2019). At Nahuelbuta these are also the elements with the lowest bio-available inventory and are thus possibly present in concentrations below equilibrium there.

The third possibility is that the inventory of a bio-available nutrient pool is set by the rate at which an element is extracted into plants from regolith relative to its replenishment by weathering. For a given bio-available reservoir an increase in uptake rate (Fig. 4; Table 3) will decrease the turnover time, or residence time of mineral-derived nutrients in the soil bio-available fraction ($T^{X}_{bio-av.soil,U}$; Table 8). For all important mineral nutrients, we see a decrease in turnover time of the bio-available soil pool with respect to uptake from the arid to the humid sites. Short turnover times with respect to uptake also reflect fast recycling. The humid-temperate ecosystem in the south of our ecological gradient is dominated by this "organic nutrient cycle".

Yet the organic nutrient cycle alone cannot be separated from its geogenic counterpart, because as discussed above the regolith nutrient pool is subject to losses by desorption and runoff, and these we consider to be quantified by the elemental weathering release flux $W^{X}_{regolith}$. Another loss trajectory not included in $W^{X}_{regolith}$ might be erosion of solid plant matter (Uhlig et al., 2017).

https://doi.org/10.5194/bg-2020-69
Preprint. Discussion started: 9 March 2020

To prevent the bio-available nutrient stocks from eventually running into depletion over longer timescales, the pool needs to be replenished. This replenishment takes place either by exogenous inputs (e.g. Boy and Wilcke, 2008; Porder et al., 2007; Vitousek, 2004; Vitousek et al., 2010), or by weathering of primary minerals at depth (Uhlig et al., 2017; Uhlig and von Blanckenburg, 2019). This replenishment is the "geogenic nutrient pathway". In the arid Pan de Azúcar, where weathering-release fluxes are low, these pools are being substantially replenished by the deposition of atmospheric sources (up to 93%; Table 6). In the other study sites the bio-available pools are being replenished by weathering of rock and regolith. The timescales $T^{X}_{bio-av.soil,W}$ over which this replenishment from weathering occurs do not deviate much between semi-arid, mediterranean, and humid-temperate climates, bar a few exceptions (Table 8). For Ca, Mg, and Sr these turnover times are within the same range as turnover times with respect to plant uptake, meaning these elements reflect a delicate balance between supply and nutrient demand. For P and K they are sometimes orders of magnitude longer than their turnover times with respect to plant uptake. For example, the inventory of K in the bio-available soil pool at Nahuelbuta is turned over every 30 years between soil and plants, but it takes 400 years to replenish their external losses by weathering. The turnover times of the bio-available fraction in saprolite with respect to weathering (calculated here for an inventory of the uppermost meter), decrease from the semi-arid, mediterranean, to the humid-temperate site for the elements Ca, Mg, K, and Sr (but not for P). The weathering turnover times in the south are lower because of the lower bio-available inventories, given that supply rates by weathering do not differ as much as the inventories.

A key observation of these considerations is the decrease in the saprolites' bio-available pool in K, Mg, and Ca from the dry to wet sites, the increase in the organic nutrient cycle as reflected by decreasing turnover times with respect to plant uptake and increasing recycling ratios, all in the face of similar weathering supply rates of nutrients. We speculate that soil chemical properties and water discharge are of subordinate importance in setting the size of the bio-available regolith pool. Instead, we consider plants and their nutrient demands to primarily control its size. If true, biological mechanisms need to be in place that regulate this delicate balance between nutrient replenishment by weathering and plant uptake in the ecosystems of Santa Gracia, La Campana, and Nahuelbuta, in order to prevent the nutrient pools from entire depletion.

5.5 Is weathering modulated by biota?

According to the conventional paradigm one would expect high weathering-release fluxes at sites at which MAP and hence runoff is high because weathering rate is proportional to runoff for the chemostatic elements that comprise the bulk of the weathering flux, amongst them Si that contributes roughly half of the flux (e.g. Godsey et al., 2019; Maher and Chamberlain, 2014). High NPP is thought to raise $W^{X}_{regolith}$ as well (e.g. Berner et al., 2003; Brantley et al., 2011; Buss et al., 2005; Kelly et al., 1998; Porder, 2019; Schwartzmann, 2015). Indeed, plants and their associated micro-biota do enhance weathering rates in a direct and indirect way. (1) Deep plant roots can increase regolith thickness (Brantley et al., 2017). (2) Land plants regulate the hydrological cycle and hence modulating runoff and total weathering fluxes (Drever and Zobrist, 1992). (3) Ectomycorrhizal fungi can actively extract nutrients such as P, K, Ca, Mg, and Fe from minerals (Finlay et al., 2009;

https://doi.org/10.5194/bg-2020-69
Preprint. Discussion started: 9 March 2020

Rosenstock, 2009; Rosling et al., 2004) distant from the root, and even during dry conditions and thereby increase mineral dissolution kinetics. (4) Through the respiratory release of soil CO_2 and excretion of organic complexing agents plants, hyphae and their associated microbiota can increase the solubility limits of cations by a factor of up to <10 (Winnick and Maher, 2018). However, we see no increase in weathering rate along the MAP and NPP gradient, and, with the exception of arid Pan de Azúcar, not even an increase in weathering intensity as denoted by CDF (Fig. 3) or the depletion (τ) of Ca, Mg, or K (Fig. A1). These indices are similar between the other three sites even though they are sensitive indicators of primary mineral dissolution. We are faced with the situation that the increased plant cover and NPP not only fails to accelerate weathering. We speculate that the effect of vegetation might even compensate for a potential increase in weathering that would be caused by the increase in MAP, essentially damping the geogenic pathway.

To evaluate why biota and runoff do not accelerate weathering, we focus on the two study sites in semi-arid (Santa Gracia) and humid-temperate climate (Nahuelbuta). In these sites, soil weathering rates (5 – 10 t km^{-2} yr^{-1}; Table 1) and weathering-release fluxes ($W^{X}_{regolith}$; Fig. 4, Table 3) of most nutrients are on par despite massive differences in vegetation cover, primary productivity (NPP), and even precipitation (MAP; Table 1). By comparison, the La Campana site features higher weathering rates simply because of its steeper topography denudation rates are higher (e.g. Oeser et al., 2018; Schaller et al., 2018; van Dongen et al., 2019). We evaluate bio-weathering by the interactions (1) to (4) introduced above.

(1) Roots deepening regolith thickness. While a detailed survey of rooting depth along the EarthShape gradient has not been done, deep roots were not observed in Santa Gracia whereas in (La Campana and) Nahuelbuta individual roots reached up to several meters depth into saprolite. A and B horizons in Santa Gracia are shallow (20 – 40 cm), whereas they are deep in Nahuelbuta (80 – 100 cm; Oeser et al., 2018; Bernhard et al., 2018). We do not know the depth of the weathering front which appears to be at least a dozen of meters depth or more at both sites. Thus, deep rooting can benefit plant growth by making a higher nutrient inventory available.

(2) Canopy and roots converting precipitation into evapotranspiration. In sites with higher vegetation cover, water vapor is being recycled and does not immediately enter runoff. By providing canopy, trees can modulate infiltration whereas they turn water back into transpiration (Ibarra et al., 2019). For example Ibarra et al. (2019) have shown that total runoff can decrease by up to 23% as vegetation cover raise from barely vegetated towards highly vegetated sites. Such an effective water recycling hence decreases total runoff and potentially reduces weathering-release fluxes in the highly vegetated sites of La Campana and Nahuelbuta. However, along the EarthShape transect this potential total 23% reduction is a minor effect when considering the 100-fold increase in precipitation over the entire gradient. A larger effect might be presented by roots if they provide preferential flowpaths such that infiltrating water either bypasses the regolith matrix available for weathering (Brantley et al., 2017). However, given the deep weathering front at the EarthShape sites that is likely beneath rooting depth we consider this effect to be minor too, or in the contrary might even increase deep weathering. Thus, we consider the impact of plants on the hydrology that is relevant to weathering to be minor along the EarthShape gradient.

(3) Increase in primary mineral dissolution by ectomycorrhizal fungi. As yet we have no direct observations on nutrient foraging by fungi and other microbes in regolith from the EarthShape sites as obtained on other mountain sites in Chile (Godoy

https://doi.org/10.5194/bg-2020-69
Preprint. Discussion started: 9 March 2020

and Mayr, 1989). Parameters of total microbial biomass in saprolite show no increase along the gradient: total gene copy have similar ranges from Santa Gracia to Nahuelbuta, and DNA amounts even decrease slightly (Oeser et al., 2018). Common strategies of microbial symbionts by tree roots suggest that energy investment into nutrient recycling from leaf litter is more advantageous than dissolving primary mineral (Andrino et al., 2019). Thus, we would expect that mycorrhiza predominantly aids recycling in La Campana and Nahuelbuta. In Santa Gracia, however, the absence of a litter layer may prompt the subsurface fungal network to invest into primary mineral dissolution, adding microbial weathering to total weathering at that that site.

(4) Increasing solubility by release of soil CO_2 and organic complexing agents. Process (4) mainly increases the equilibrium limit of elemental solubility. If dissolution is not kinetically limited, we would indeed expect higher solute concentrations with higher soil CO_2, and hence higher dissolution rates of primary minerals (Winnick and Maher, 2018). Plants potentially impose a negative feedback onto this dependence by interfering into the silicon cycle. Because silicon is the most abundant element in felsic rock and regolith (besides oxygen) it exerts the major control on the total weathering fluxes. The conversion of dissolved silicon into biosilica by uptake formation of e.g. phytoliths would aid kaolinite formation (Lucas, 2001). However, the Si uptake flux at all sites is negligible compared to the Si weathering flux: $W^{Si}_{regolith}$ amounts to 2100 and 2000 mg m^{-2} yr^{-1} in Santa Gracia and Nahuelbuta, respectively (Table 3). Si concentration in the above-ground living ecosystem of Santa Gracia (1400 µg g^{-1}) exceeds the Si concentration in Nahuelbuta (110 µg g^{-1}; Table 5). This leads to an uptake of Si from soil solution (U^{Si}_{total}) of 100 mg m^{-2} yr^{-1} in Santa Gracia and 30 mg m^{-2} yr^{-1} in Nahuelbuta (Table 3) which is only 2 – 5% of the Si release flux. We can therefore exclude plant Si uptake and recycling of Si as a factor impacting weathering rates. A key observation is provided by the analysis of pedogenic oxides (i.e. dithionite-extractable Al, Si extracted by oxalate, dithionite, and pyrophosphate; Oeser et al., 2018) and cation exchange capacity (Bernhard et al., 2018). These analyses suggest high amounts of amorphous precipitates and secondary minerals in the regolith of Nahuelbuta but not in Santa Gracia. We thus argue that Si is effectively captured in these barely soluble secondary minerals and in turn, $W^{Si}_{regolith}$ in Nahuelbuta is subdued in spite of elevated solubility of primary minerals due to increased CO_2 respiration by roots.

Ecosystems thus exert substantial control over weathering by both directly and indirectly modulating processes. These processes can either enhance or reduce weathering fluxes and result, in combination with effective recycling loops of plant-litter material, in well-balanced nutrient cycles. The silicate weathering fluxes become effectively decoupled from the ultimate nutrient demands of biota. Our empirical evidence provided here suggests that the combination of recycling and negative feedbacks on weathering by secondary solid formation within the regolith counterbalance weathering rates in areas of high vegetation and biomass growth from what they would be in the absence of high biomass density.

6 Conclusions

We found that even though the four EarthShape study sites feature a steep north-south gradient in MAP and NPP, none such a gradient was apparent for weathering rates and weathering intensity between the study sites situated in semi-arid,

https://doi.org/10.5194/bg-2020-69
Preprint. Discussion started: 9 March 2020

mediterranean, and humid-temperate climate. Thus, the ecosystems with high NPP maintain their nutrient supply by increasing recycling rather than increasing weathering. We consequently find that the "organic nutrient pathway" intensifies, whereas the "geogenic nutrient pathway" stays steady despite increasing MAP and NPP.

Ecological stoichiometry in plants and Sr isotopes reflects the bio-available fraction in saprolite and soil. At the sites with high NPP, the bio-available fraction approaches a plant-dominated ecological stoichiometry signature by intense recycling. Besides nitrogen, the first mineral nutrient to be limit plant growth might be K rather than P. However, we found that deep-rooting plants can bypass this shortage K in the upper regolith by deep K-uptake from beneath the regolith profiles.

In fact, the presence of plants might compensate a potential weathering increase along the gradient downward by regulating the hydrological cycle, fostering secondary mineral formation, and a microbial community specializing on nutrient-recycling rather than nutrient-acquisition through weathering. Due to this nutrient buffering by recycling, higher plants today may not be a big driver in the global silicate-weathering cycle.

7 Appendices

Appendix A: Calculation of fluxes and inventories in terrestrial ecosystems

Weathering indices (CDF & τ)

Zr, Ti, and Nb are commonly used to estimate mass losses to the dissolved form during weathering (Eqs. 5 & 6) as they are presumed to be the least mobile elements during weathering (Chadwick et al., 1990; White et al., 1998). The suitability of these elements for the EarthShape study sites has been evaluated and thoroughly discussed on a site to site basis in Oeser et al. (2018). Based on possible Ti-mobility in some samples and the fact that Zr is used as a reference element in the majority of weathering and soil production studies worldwide (e.g. Fisher et al., 2017; Green et al., 2006; Hewawasam et al., 2013; Riebe and Granger, 2013; Riebe et al., 2001; Schuessler et al., 2018; Uhlig et al., 2017), Zr was taken as immobile reference element in this study.

The calculations of these weathering indices rely on a good approximation of the regolith profiles' initial substrate (i.e. chemical bedrock composition). Thus, any regolith sample with a Zr concentration that was lower than the mean of unweathered bedrock by more than one standard deviation (1SD) was excluded from further consideration. These samples potentially originate from a chemically distinct bedrock or highlight another type of substrate heterogeneity (e.g. a pegmatitic vein) as a lower Zr concentration cannot be due to weathering. Saprolite samples were also excluded from our data set if Cr and Ti concentrations were twice those of unweathered bedrock (+ 1SD). Elevated concentrations of these elements imply the presence of mafic precursor rock such as commonly present in bedrocks' mafic enclaves. All such excluded samples are marked grey in Figs. 3 & A1.

https://doi.org/10.5194/bg-2020-69
Preprint. Discussion started: 9 March 2020

The concentration of K throughout the entire regolith profiles in Santa Gracia is three-fold higher than K contained in local bedrock samples (Oeser et al., 2018). We thus assume that the K concentration in the bedrock samples of Santa Gracia as determined by Oeser et al. (2018) underestimates the actually occurring K concentration of local bedrock. Thus, τ^{K} has been calculated using published values on K and Zr concentration from a study nearby (Miralles González, 2013).

Weathering fluxes

To estimate elemental release fluxes from regolith (Eq. 3) for each study site, the most negative τ-values from the shallowest mineral-soil sample of each regolith profile were used (red-circled symbols in Fig. A1), resulting in an integrated net-elemental release over each entire regolith profile. Ultimately, the elemental chemical weathering flux ($W^{X}_{regolith}$) at each study site has been averaged. Because some fraction of this flux might not be in the reach of the plants' roots (e.g. if a fraction is lost into deep groundwater) an upper estimate of the nutrient fluxes from rock into vegetation results. $W^{X}_{regolith}$ is reported in Table 3.

Ecosystem nutrient uptake fluxes

Total ecosystem nutrient uptake fluxes (U^{X}_{total}) have been evaluated using Eq. 4 and are reported in Table 3. Net primary productivity (NPP), has been derived from a dynamic vegetation model (LPJ-GUESS) simulating vegetation cover and composition during the Holocene (Werner et al., 2018) and is reported in Table 1. Biomass production was estimated from NPP(C) by assuming that dry biomass consists of 50 wt% carbon. To obtain the element-specific uptake rate U^{X} $GrowthRate_{Plant}$ is multiplied with the bulk concentration of X in the plants $[X]_{Plant}$. To estimate an elemental bulk ecosystem composition, we applied the dimensionless organ growth quotients GL/GS (leaf growth relative to stem growth) and GL/GR (leaf growth relative to root growth) in accordance with Niklas and Enquist (2002). However, the sampling and analyses of roots was excluded in this study, because of the difficulties that arose in associating roots to a specific tree or shrub. For elemental analysis this difficulty is compounded by the difficulties encountered during the roots' purification from soil particles. We thus adapted the organ growth quotients from the work of Niklas and Enquist (2002), such that we only differentiate between the growth rate of leaves and stem, respectively, and the differences of these quotients between angiosperms and gymnosperms. Ultimately, elemental bulk ecosystem composition (Table 5) has been determined by weighting the averaged elemental composition for each sampled plant for their relative abundance in the respective ecosystem.

Inventories

The inventories for the bio-available fraction ($I^{X}_{bio\text{-}av.}$) and in bulk regolith (I^{X}_{bulk}) have been calculated using Eq. 8 and are reported in Table 4. $I^{X}_{bio\text{-}av.}$ was determined for both the bio-available fraction in soil (comprised of the A and B horizon; $I^{X}_{bio\text{-}av,\,soil}$) and saprolite ($I^{X}_{bio\text{-}av,\,sap}$). For the calculation of all inventories we used the soils' bulk density determined by

https://doi.org/10.5194/bg-2020-69
Preprint. Discussion started: 9 March 2020


Biogeosciences Discussions

Bernhard et al. (2018). I^X_{bulk} is comprised of elements contained in fine-earth material and in fragmented rocks and coarse material (e.g. core stones). We derive the relative amount of coarse material of each depth increment from Bernhard et al. (2018) and allocate them the bedrocks' chemical composition (Table S1). If information on either bulk density or the relative amount of coarse material was not available, the respective horizons' average has been used for the calculation of $I^X_{i,j}$.

Ultimately, we do not know how far the saprolite extents to depth in each of the eight regolith profiles. Thus, for comparison purposes, we calculated the inventories of the bio-available fraction in saprolite ($I^X_{bio\text{-}av,\,sap}$) and in bulk regolith ($I^X_{bulk}$) to the depth of the respective regolith profile and normalized this value to the arbitrary value of 1 m.

Nutrient recycling factor

The nutrient recycling factor Rec^X was calculated using Eq. 7 and is reported in Table 7. This factor, however, might represent an underestimate as it is parameterized with $W^X_{regolith}$ and some fraction of which will bypass nutrient uptake by plants if it is drained directly via groundwater into streams. Moreover, Rec^X might also be underrated for some elements as it does not account for stem-flow fluxes and throughfall. According to e.g. Wilcke et al. (2017), these fluxes are generally highest for K compared to other plant-essential elements.

In Pan de Azúcar, where atmospheric deposition (Dep^X_{dry} and Dep^X_{wet}) has been reported (e.g. increasing τ-values towards the profiles top despite bio-lifting of elements and field observation; Oeser et al., 2018) we need to consider these inputs in addition to the weathering release fluxes ($W^X_{regolith}$). Thus, to account for all potential sources of elements available for plant uptake, the nutrient recycling factor in Pan de Azúcar has been determined using:

$$Rec^X = \frac{U^X_{total}}{W^X_{regolith} + Dep^X_{wet} + Dep^X_{dry}}$$

Atmospheric deposition fluxes have been estimated by determining the absolute difference between the lowest τ-value in the shallowest mineral-soil sample and the highest τ-value in the soil profile above it. Further, we assume that elemental gains (i.e. increasing τ-values) in the regolith profiles are attributed solely to atmospheric deposition. We test these estimates for atmospheric depositional fluxes by placing the elemental gains in proportion to the initially determined weathering release fluxes ($W^X_{regolith}$, Eq. 3; Table 3).

Uncertainty estimation on nutrient fluxes

The uncertainties on the nutrient fluxes of $W^X_{regolith}$ and U^X_{total} were estimated performing Monte Carlo simulations in which 20 000 random data sets were sampled within the standard deviation of all input parameters using a Box-Muller transformation (Box and Muller, 1958). The uncertainties used for the simulation were the SD of $W^X_{regolith}$, the respective regolith profile's denudation rate (D, Table 1), the SD of the bedrocks' element concentration of interest, and 3% relative uncertainty on the

https://doi.org/10.5194/bg-2020-69
Preprint. Discussion started: 9 March 2020

element concentration in regolith samples. In the case of U^{X}_{total} the SD of the respective study site's NPP and the SD of the chemical composition of the weighted plants (Table 5) were used.

8 Sample availability

All sample metadata are already available on a public server using unique sample identifiers in form of the "International Geo Sample Number" (IGSN).

9 Author contributions

R.A. Oeser conducted field sampling, analyzed samples, interpreted data, and wrote text. F. von Blanckenburg designed the study, selected the study sites, interpreted data, and wrote text.

10 Competing financial interests

The authors declare no competing financial interests.

11 Additional information

Supplementary data tables are available at GFZ data services (Oeser and von Blanckenburg, 2020).

12 Acknowledgements

We acknowledge CONAF in Chile for providing us with the opportunity to work in the national parks of Pan de Azúcar, La Campana, and Nahuelbuta. We also thank CEAZA for facilitating access to the Reserva Natural Santa Gracia. We are grateful to J. Boy (Soil Sciences, Leibniz Universität Hannover, Germany) for discussions, and D. Uhlig (Institute of Bio- and Geosciences, Forschungszentrum Jülich, Germany), Michaela Dippold (Department of Crop Sciences, Georg-August University Goettingen, Germany), and Matthew Winnick (Department of Geosciences, University of Massachusetts, USA) for informal reviews of an earlier text version. R.A. Oeser and F. von Blanckenburg are grateful for funding by the German National Science Foundation Priority Program DFG-SPP 1803 (EarthShape; www.earthshape.net). We thank Leandro Paulino (Departamento de Suelos y Recursos Naturales, Universitad de Concepción, Chile) and Kirstin Übernickel for managing the priority program and Todd Ehlers (both Institute for Geosciences, Universität Tübingen, Germany) for its co-coordination.

https://doi.org/10.5194/bg-2020-69
Preprint. Discussion started: 9 March 2020

13 References

Amundson, R., Richter, D. D., Humphreys, G. S., Jobbágy, E. G., and Gaillardet, J. r. m.: Coupling between Biota and Earth Materials in the Critical Zone, Elements, 3, 327-332, 10.2113/gselements.3.5.327, 2007.

Andrino, A., Boy, J., Mikutta, R., Sauheitl, L., and Guggenberger, G.: Carbon Investment Required for the Mobilization of Inorganic and Organic Phosphorus Bound to Goethite by an Arbuscular Mycorrhiza (Solanum lycopersicum x Rhizophagus irregularis), Frontiers in Environmental Science, 7, 10.3389/fenvs.2019.00026, 2019.

Armesto, J. J., Vidiella, P. E., and Gutiérrez, J. R.: Plant communities of the fog-free coastal desert of Chile: plant strategies in a fluctuating environment., Revista Chilena de Historia Natural, 66, 271-282, 1993.

Arunachalam, J., Emons, H., Krasnodebska, B., and Mohl, C.: Sequential extraction studies on homogenized forest soil samples, The Science of the Total Environment, 181, 147-159, 1996.

Bahre, C. J.: Destruction of the natural vegetation of north-central Chile, Univ of California Press, 1979.

Baskaran, P., Hyvonen, R., Berglund, S. L., Clemmensen, K. E., Agren, G. I., Lindahl, B. D., and Manzoni, S.: Modelling the influence of ectomycorrhizal decomposition on plant nutrition and soil carbon sequestration in boreal forest ecosystems, New Phytol, 213, 1452-1465, 10.1111/nph.14213, 2017.

Beerling, D. J., and Berner, R. A.: Feedbacks and the coevolution of plants and atmospheric CO2, Proc Natl Acad Sci U S A, 102, 1302-1305, 10.1073/pnas.0408724102, 2005.

Berg, K., and Breitkreuz, C.: Mesozoische Plutone in der nordchilenischen Küstenkordillere: petrogenese, geochronologie, Geochemie und Geodynamik mantelbetonter Magmatite, Geotectonic Research, 66, Schweizerbart Science Publishers, 1983.

Berg, K., and Baumann, A.: Plutonic and metasedimentary rocks from the Coastal Range of northern Chile: Rb-Sr and U-Pb isotopic systematics, Earth and Planetary Science Letters, 75, 101-115, 1985.

Berner, E. K., Berner, R. A., and Moulton, K. L.: Plants and Mineral Weathering: Present and Past, in: Treatise on Geochemistry, 169-188, 2003.

Bernhard, N., Moskwa, L.-M., Schmidt, K., Oeser, R. A., Aburto, F., Bader, M. Y., Baumann, K., von Blanckenburg, F., Boy, J., van den Brink, L., Brucker, E., Canessa, R., Dippold, M. A., Ehlers, T. A., Fuentes, J. P., Godoy, R., Köster, M., Kuzyakov, Y., Leinweber, P., Neidhard, H., Matus, F., Mueller, C. W., Oelmann, Y., Oses, R., Osses, P., Paulino, L., Schaller, M., Schmid, M., Spielvogel, S., Spohn, M., Stock, S., Stroncik, N., Tielbörger, K., Übernickel, K., Scholten, T., Seguel, O., Wagner, D., and Kühn, P.: Pedogenic and microbial interrelations to regional climate and local topography: new insights from a climate gradient (arid to humid) along the Coastal Cordillera of Chile, Catena, 170, 10.1016/j.catena.2018.06.018, 2018.

Blanco-Chao, R., Pedoja, K., Witt, C., Martinod, J., Husson, L., Regard, V., Audin, L., Nexer, M., Delcaillau, B., Saillard, M., Melnick, D., Dumont, J. F., Santana, E., Navarrete, E., Martillo, C., Pappalardo, M., Ayala, L., Araya, J. F., Feal-Perez, A., Correa, D., and Arozarena-Llopis, I.: The rock coast of South and Central America, in: Rock Coast Geomorphology: A Global Synthesis., 1, The Geological Society, London, 155-191, 2014.

Blum, J. D., Klaue, A., Nezat, C. A., Driscoll, C. T., Johnson, C. E., Siccama, T. G., Eagar, C., Fahey, T. J., and Likens, G. E.: Mycorrhizal weathering of apatite as an important calcium source in base-poor forest ecosystems, Nature, 417, 729-731, 10.1038/nature00793, 2002.

Blum, J. D., Hamburg, S. P., Yanai, R. D., and Arthur, M. A.: Determination of foliar Ca/Sr discrimination factors for six tree species and implications for Ca sources in northern hardwood forests, Plant and Soil, 356, 303-314, 10.1007/s11104-011-1122-2, 2012.

Box, G. E. P., and Muller, M. E.: A note on the generation of random normal deviates, Ann. Math. Statist., 29, 610-611, 10.1214/aoms/1177706645, 1958.

Boy, J., and Wilcke, W.: Tropical Andean forest derives calcium and magnesium from Saharan dust, Global Biogeochem Cy, 22, n/a-n/a, 10.1029/2007gb002960, 2008.

Brantley, S. L., and Lebedeva, M.: Learning to Read the Chemistry of Regolith to Understand the Critical Zone, Annual Review of Earth and Planetary Sciences, 39, 387-416, 10.1146/annurev-earth-040809-152321, 2011.

Brantley, S. L., Megonigal, J. P., Scatena, F. N., Balogh-Brunstad, Z., Barnes, R. T., Bruns, M. A., Van Cappellen, P., Dontsova, K., Hartnett, H. E., Hartshorn, A. S., Heimsath, A., Herndon, E., Jin, L., Keller, C. K., Leake, J. R., McDowell, W. H., Meinzer, F. C., Mozdzer, T. J., Petsch, S., Pett-Ridge, J., Pregitzer, K. S., Raymond, P. A., Riebe, C. S., Shumaker, K., Sutton-Grier, A., Walter, R., and Yoo, K.: Twelve testable hypotheses on the geobiology of weathering, Geobiology, 9, 140-165, 10.1111/j.1472-4669.2010.00264.x, 2011.

Brantley, S. L., Lebedeva, M., and Heimshath, E. H.: A Geobiological View of Weathering and Erosion, in: Fundamentals of Geobiology, edited by: Knoll, A. H., Blackwell Publishing, 2012.

Brantley, S. L., Eissenstat, D. M., Marshall, J. A., Godsey, S. E., Balogh-Brunstad, Z., Karwan, D. L., Papuga, S. A., Roering, J., Dawson, T. E., Evaristo, J., Chadwick, O., McDonnell, J. J., and Weathers, K. C.: Reviews and syntheses: on the roles trees play in building and plumbing the critical zone, Biogeosciences, 14, 5115-5142, 10.5194/bg-14-5115-2017, 2017.

Brucker, E., and Spohn, M.: Formation of soil phosphorus fractions along a climate and vegetation gradient in the Coastal Cordillera of Chile, Catena, 180, 203-211, 10.1016/j.catena.2019.04.022, 2019.

Buendía, C., Kleidon, A., and Porporato, A.: The role of tectonic uplift, climate, and vegetation in the long-term terrestrial phosphorous cycle, Biogeosciences, 7, 2025-2038, 10.5194/bg-7-2025-2010, 2010.

https://doi.org/10.5194/bg-2020-69
Preprint. Discussion started: 9 March 2020

Bullen, T. D., and Chadwick, O.: Ca, Sr and Ba stable isotopes reveal the fate of soil nutrients along a tropical climosequence in Hawaii, Chemical Geology, 422, 25-45, 10.1016/j.chemgeo.2015.12.008, 2016.
Buss, H. L., Bruns, M. A., Schultz, D. J., Moore, J., Mathur, C. F., and Brantley, S. L.: The coupling of biological iron cycling and mineral weathering during saprolite formation, Luquillo Mountains, Puerto Rico, Geobiology, 3, 247-260, 2005.
Calmels, D., Gaillardet, J., and François, L.: Sensitivity of carbonate weathering to soil CO2 production by biological activity along a temperate climate transect, Chemical Geology, 390, 74-86, 2014.
Canadell, J., Jackson, R., Ehleringer, J., Mooney, H., Sala, O., and Schulze, E.-D.: Maximum rooting depth of vegetation types at the global scale, Oecologia, 108, 583-595, 1996.
Capek, P., Manzoni, S., Kastovska, E., Wild, B., Diakova, K., Barta, J., Schnecker, J., Biasi, C., Martikainen, P. J., Alves, R. J. E., Guggenberger, G., Gentsch, N., Hugelius, G., Palmtag, J., Mikutta, R., Shibistova, O., Urich, T., Schleper, C., Richter, A., and Santruckova, H.: A plant-microbe interaction framework explaining nutrient effects on primary production, Nat Ecol Evol, 10.1038/s41559-018-0662-8, 2018.
Chadwick, K. D., and Asner, G. P.: Tropical soil nutrient distributions determined by biotic and hillslope processes, Biogeochemistry, 127, 273-289, 10.1007/s10533-015-0179-z, 2016.
Chadwick, O. A., Brimhall, G. H., and Hendricks, D. M.: From a black to a gray box — a mass balance interpretation of pedogenesis, Geomorphology, 3, 369-390, 10.1016/0169-555x(90)90012-f, 1990.
Chadwick, O. A., Derry, L. A., Vitousek, P. M., Huebert, B. J., and Hedin, L. O.: Changing sources of nutrients during four million years of ecosystem development, Nature, 397, 491-497, 1999.
Chapin III, F. S.: The mineral nutrition of wild plants, Annual review of ecology and systematics, 11, 233-260, 1980.
Chapin III, F. S., Matson, P. A., and Vitousek, P. M.: Principles of Terrestrial Ecosystem Ecology, 2nd ed., 2011.
Chaudhuri, S., Clauer, N., and Semhi, K.: Plant decay as a major control of river dissolved potassium: A first estimate, Chemical Geology, 243, 178-190, 10.1016/j.chemgeo.2007.05.023, 2007.
Cleveland, C. C., and Liptzin, D.: C:N:P stoichiometry in soil: is there a “Redfield ratio” for the microbial biomass?, Biogeochemistry, 85, 235-252, 10.1007/s10533-007-9132-0, 2007.
Cleveland, C. C., Houlton, B. Z., Smith, W. K., Marklein, A. R., Reed, S. C., Parton, W., Del Grosso, S. J., and Running, S. W.: Patterns of new versus recycled primary production in the terrestrial biosphere, Proc Natl Acad Sci U S A, 110, 12733-12737, 10.1073/pnas.1302768110, 2013.
Dal Bo, I., Klotzsche, A., Schaller, M., Ehlers, T. A., Kaufmann, M. S., Fuentes Espoz, J. P., Vereecken, H., and van der Kruk, J.: Geophysical imaging of regolith in landscapes along a climate and vegetation gradient in the Chilean coastal cordillera, Catena, 180, 146-159, 10.1016/j.catena.2019.04.023, 2019.
Day, T. A., Guénon, R., and Ruhland, C. T.: Photodegradation of plant litter in the Sonoran Desert varies by litter type and age, Soil Biology and Biochemistry, 89, 109-122, 10.1016/j.soilbio.2015.06.029, 2015.
Delhaize, E., and Ryan, P. R.: Aluminum Toxicity and Tolerance in Plants, Plant Physiology, 107, 315-321, 1995.
Dere, A. L., White, T. S., April, R. H., Reynolds, B., Miller, T. E., Knapp, E. P., McKay, L. D., and Brantley, S. L.: Climate dependence of feldspar weathering in shale soils along a latitudinal gradient, Geochimica et Cosmochimica Acta, 122, 101-126, 10.1016/j.gca.2013.08.001, 2013.
Dixon, J. L., Hartshorn, A. S., Heimsath, A. M., DiBiase, R. A., and Whipple, K. X.: Chemical weathering response to tectonic forcing: A soils perspective from the San Gabriel Mountains, California, Earth and Planetary Science Letters, 323-324, 40-49, 10.1016/j.epsl.2012.01.010, 2012.
Dosseto, A., Buss, H. L., and Suresh, P. O.: Rapid regolith formation over volcanic bedrock and implications for landscape evolution, Earth and Planetary Science Letters, 337-338, 47-55, 10.1016/j.epsl.2012.05.008, 2012.
Doughty, C. E., Taylor, L. L., Girardin, C. A. J., Malhi, Y., and Beerling, D. J.: Montane forest root growth and soil organic layer depth as potential factors stabilizing Cenozoic global change, Geophysical Research Letters, 41, 983-990, 10.1002/2013gl058737, 2014.
Drever, J. I., and Zobrist, J.: Chemical weathering of silicate rocks as a function of elevation in the southern Swiss Alps, Geochimica et Cosmochimica Acta, 56, 3209-3216, 10.1016/0016-7037(92)90298-w, 1992.
Drever, J. I.: The effect of land plants on weathering rates of silicate minerals, Geochimica et Cosmochimica Acta, 58, 2325-2332, 10.1016/0016-7037(94)90013-2, 1994.
Eger, A., Yoo, K., Almond, P. C., Boitt, G., Larsen, I. J., Condron, L. M., Wang, X., and Mudd, S. M.: Does soil erosion rejuvenate the soil phosphorus inventory?, Geoderma, 332, 45-59, 10.1016/j.geoderma.2018.06.021, 2018.
Egli, M., Mirabella, A., Sartori, G., and Fitze, P.: Weathering rates as a function of climate: results from a climosequence of the Val Genova (Trentino, Italian Alps). Geoderma, 111, 99-121, 2003.
Elser, J. J., Fagan, W. F., Kerkhoff, A. J., Swenson, N. G., and Enquist, B. J.: Biological stoichiometry of plant production: metabolism, scaling and ecological response to global change, The New phytologist, 186, 593-608, 10.1111/j.1469-8137.2010.03214.x, 2010.
Faure, G., and Powell, J. L.: Strontium Isotope Geology, Isotopes in Geology, 1972.
Faure, G., and Mensing, T. M.: Isotopes: principles and applications, Wiley-Blackwell, 2005.

https://doi.org/10.5194/bg-2020-69
Preprint. Discussion started: 9 March 2020

Ferrier, K. L., Kirchner, J. W., and Finkel, R. C.: Weak influences of climate and mineral supply rates on chemical erosion rates: Measurements along two altitudinal transects in the Idaho Batholith, Journal of Geophysical Research: Earth Surface, 117, n/a-n/a, 10.1029/2011jf002231, 2012.

Finlay, R., Wallander, H., Smits, M., Holmstrom, S., van Hees, P., Lian, B., and Rosling, A.: The role of fungi in biogenic weathering in boreal forest soils, Fungal Biology Reviews, 23, 101-106, 10.1016/j.fbr.2010.03.002, 2009.

Fisher, B. A., Rendahl, A. K., Aufdenkampe, A. K., and Yoo, K.: Quantifying weathering on variable rocks, an extension of geochemical mass balance: Critical zone and landscape evolution, Earth Surface Processes and Landforms, 42, 2457-2468, 10.1002/esp.4212, 2017.

Gallo, M. E., Sinsabaugh, R. L., and Cabaniss, S. E.: The role of ultraviolet radiation in litter decomposition in arid ecosystems, Applied Soil Ecology, 34, 82-91, 10.1016/j.apsoil.2005.12.006, 2006.

Geider, R. J., and La Roche, J.: Redfield revisited: variability of C [ratio] N [ratio] P in marine microalgae and its biochemical basis, European Journal of Phycology, 37, 1-17, 10.1017/S0967026201003456, 2002.

Giehl, R. F., and von Wiren, N.: Root nutrient foraging, Plant Physiol, 166, 509-517, 10.1104/pp.114.245225, 2014.

Godoy, R., and Mayr, R.: Caracterización morfológica de micorrizas vesículo-arbusculares en coníferas endémicas del sur de Chile., Bosque, 10, 89-98, 1989.

Godsey, S. E., Hartmann, J., and Kirchner, J. W.: Catchment chemostasis revisited: Water quality responds differently to variations in weather and climate, Hydrological Processes, 33, 3056-3069, 10.1002/hyp.13554, 2019.

Green, E., Dietrich, W., and Banfield, J.: Quantification of chemical weathering rates across an actively eroding hillslope, Earth and Planetary Science Letters, 242, 155-169, 10.1016/j.epsl.2005.11.039, 2006.

Hahm, W. J., Riebe, C. S., Lukens, C. E., and Araki, S.: Bedrock composition regulates mountain ecosystems and landscape evolution, Proc Natl Acad Sci U S A, 111, 3338-3343, 10.1073/pnas.1315667111, 2014.

Hasenmueller, E. A., Gu, X., Weitzman, J. N., Adams, T. S., Stinchcomb, G. E., Eissenstat, D. M., Drohan, P. J., Brantley, S. L., and Kaye, J. P.: Weathering of rock to regolith: The activity of deep roots in bedrock fractures, Geoderma, 300, 11-31, 10.1016/j.geoderma.2017.03.020, 2017.

He, X. T., Logan, T. J., and Traina, S. J.: Physical and chemical characteristics of selected US municipal solid waste composts., Journal of Environmental Quality, 24, 543-552, 10.2134/jeq1995.00472425002400030022x, 1995.

Heartsill Scalley, T., Scatena, F. N., Moya, S., and Lugo, A. E.: Long-term dynamics of organic matter and elements exported as coarse particulates from two Caribbean montane watersheds, Journal of Tropical Ecology, 28, 127-139, 10.1017/s0266467411000733, 2012.

Hervé, F., Munizaga, F., Mantovani, M., and Hervé, M.: Edades Rb/Sr neopaleozoicas del basamento cristallino de la Cordillera de Nahuelbuta, Primer Congresso Geologico Chileno, Santiago, 1976.

Hervé, F.: Petrology of the crystalline basement of the Nahuelbuta Mountains, south-central Chile, Comparative studies on the Geology of the Circum-Pacific orogenic belt in Japan and Chile, edited by: Ishikava, I., and Aguirre, L., Japan Society for the Promotion of Science, 1977.

Hewawasam, T., von Blanckenburg, F., Bouchez, J., Dixon, J. L., Schuessler, J. A., and Maekeler, R.: Slow advance of the weathering front during deep, supply-limited saprolite formation in the tropical Highlands of Sri Lanka, Geochimica et Cosmochimica Acta, 118, 202-230, 10.1016/j.gca.2013.05.006, 2013.

Hillebrand, H., Cowles, J. M., Lewandowska, A., Van de Waal, D. B., and Plum, C.: Think ratio! A stoichiometric view on biodiversity–ecosystem functioning research, Basic and Applied Ecology, 15, 465-474, 10.1016/j.baae.2014.06.003, 2014.

Ibarra, D. E., Rugenstein, J. K. C., Bachan, A., Baresch, A., Lau, K. V., Thomas, D. L., Lee, J.-E., Boyce, C. K., and Chamberlain, C. P.: Modeling the consequences of land plant evolution on silicate weathering, American Journal of Science, 319, 1-43, 10.2475/01.2019.01, 2019.

Jobbágy, E. G. a. J., Robert B: The distribution of soil nutrients with depth: global patterns and the imprint of plants, Biogeochemistry, 53, 51-77, 2001.

Jung, M., Reichstein, M., Margolis, H. A., Cescatti, A., Richardson, A. D., Arain, M. A., Arneth, A., Bernhofer, C., Bonal, D., Chen, J., Gianelle, D., Gobron, N., Kiely, G., Kutsch, W., Lasslop, G., Law, B. E., Lindroth, A., Merbold, L., Montagnani, L., Moors, E. J., Papale, D., Sottocornola, M., Vaccari, F., and Williams, C.: Global patterns of land-atmosphere fluxes of carbon dioxide, latent heat, and sensible heat derived from eddy covariance, satellite, and meteorological observations, Journal of Geophysical Research, 116, 10.1029/2010jg001566, 2011.

Kelly, E. F., Chadwick, O. A., and Hilinski, T. E.: The effect of plants on mineral weathering, Biogeochemistry, 42, 21-53, 10.1023/a:1005919306687, 1998.

Kleidon, A., Fraedrich, K., and Heimann, M.: A Green Planet Versus a Desert World: Estimating the Maximum Effect of Vegetation on the Land Surface Climate, Climatic Change, 44, 471-493, 10.1023/a:1005559518889, 2000.

Kronzucker, H. J., and Britto, D. T.: Sodium transport in plants: a critical review, New Phytol, 189, 54-81, 10.1111/j.1469-8137.2010.03540.x, 2011.

Kump, L. R., Brantley, S. L., and Arthur, M. A.: Chemical Weathering, Atmospheric CO2, and Climate, Annual Review of Earth and Planetary Sciences, 28, 611-667, 10.1146/annurev.earth.28.1.611, 2000.

Laliberte, E., Grace, J. B., Huston, M. A., Lambers, H., Teste, F. P., Turner, B. L., and Wardle, D. A.: How does pedogenesis drive plant diversity?, Trends Ecol Evol, 28, 331-340, 10.1016/j.tree.2013.02.008, 2013.

Lang, F., Bauhus, J., Frossard, E., George, E., Kaiser, K., Kaupenjohann, M., Krüger, J., Matzner, E., Polle, A., Prietzel, J., Rennenberg, H., and Wellbrock, N.: Phosphorus in forest ecosystems: New insights from an ecosystem nutrition perspective, Journal of Plant Nutrition and Soil Science, 179, 129-135, 10.1002/jpln.201500541, 2016.

Lee, J.-E., and Boyce, K.: Impact of the hydraulic capacity of plants on water and carbon fluxes in tropical South America, J Geophys Res, 115, 10.1029/2010jd014568, 2010.

Lenton, T. M., Crouch, M., Johnson, M., Pires, N., and Dolan, L.: First plants cooled the Ordovician, Nature Geoscience, 5, 86-89, 10.1038/ngeo1390, 2012.

Liang, Y., Sun, W., Zhu, Y. G., and Christie, P.: Mechanisms of silicon-mediated alleviation of abiotic stresses in higher plants: a review, Environ Pollut, 147, 422-428, 10.1016/j.envpol.2006.06.008, 2007.

Lucas, Y.: The Role of Plants in Controlling Rates and Products of Weathering: Importance of Biological Pumping, Annual Review of Earth and Planetary Sciences, 29, 135-163, 2001.

Luebert, F., and Pliscoff, P.: Sinópsis bioclimática y vegetacional de Chile., Editorial Universitaria, Santiago de Chile, 2006.

Maher, K., and Chamberlain, C. P.: Hydrologic regulation of chemical weathering and the geologic carbon cycle, Science, 343, 1502-1504, 10.1126/science.1250770, 2014.

Marschner, H.: General introduction to the mineral nutrition of plants, Inorganic plant nutrition, 5-60, 1983.

Melnik, D.: Rise of the central Andean coast by Earthquakes straddling the Moho., Nature Geoscience, 9, 401-407, https://doi.org/10.1038/ngeo2683, 2016.

Información Oficial Hidrometeorológica y de Calidad de Aguas en Línea: http://snia.dga.cl/BNAConsultas/reportes, access: 12.06.2017, 2017.

Minyard, M. L., Bruns, M. A., Liermann, L. J., Buss, H. L., and Brantley, S. L.: Bacterial Associations with Weathering Minerals at the Regolith-Bedrock Interface, Luquillo Experimental Forest, Puerto Rico, Geomicrobiology Journal, 29, 792-803, 10.1080/01490451.2011.619640, 2012.

Miralles González, C.: Evaluación de los factores que controllan la geoquímica de sedimentos fluviales de la cuenca del Río Elqui, Región de Coquimbo, Chile, Depeartamento de Geología, Universidad de Chile, 2013.

Molina, P. G., Parada, M. A., Gutiérrez, F. J., Ma, C., Li, J., Yuanyuan, L., Reich, M., and Aravena, Á.: Protracted late magmatic stage of the Caleu pluton (central Chile) as a consequence of heat redistribution by diking: Insights from zircon data and thermal modeling, Lithos, 227, 255-268, 10.1016/j.lithos.2015.04.008, 2015.

Mooney, H. A., Gulmon, S. L., Ehleringer, J., and Rundel, P. W.: Atmospheric water uptake by an Atacama Desert shrub, Science, 209, 693-694, 1980.

Moore, C. M., Mills, M. M., Arrigo, K. R., Berman-Frank, I., Bopp, L., Boyd, P. W., Galbraith, E. D., Geider, R. J., Guieu, C., Jaccard, S. L., Jickells, T. D., La Roche, J., Lenton, T. M., Mahowald, N. M., Marañón, E., Marinov, I., Moore, J. K., Nakatsuka, T., Oschlies, A., Saito, M. A., Thingstad, T. F., Tsuda, A., and Ulloa, O.: Processes and patterns of oceanic nutrient limitation, Nature Geoscience, 6, 701-710, 10.1038/ngeo1765, 2013.

Moore, T. R., Trofymow, J. A., Siltanen, M., Prescott, C., and Group, C. W.: Patterns of decomposition and carbon, nitrogen, and phosphorus dynamics of litter in upland forest and peatland sites in central Canada, Canadian Journal of Forest Research, 35, 133-142, 10.1139/x04-149, 2005.

Moscoso, R., Nasi, C., and Salinas, P.: Hoja Vallenar y parte norte de La Serena: regiones de Atacama y Coquimbo: carta geológica de Chile 1: 250.000, Servicio Nacional de Geología y Minería Chile, 1982.

Moulton, K. L., West, J., and Berner, R. A.: Solute flux and mineral mass balance approaches to the quantification of plant effects on silicate weathering, American Journal of Science, 300, 539-570, 10.2475/ajs.300.7.539, 2000.

Nier, A. O.: The Isotopic Constitution of Strontium, Barium, Bismuth, Thallium and Mercury, Physical Review, 54, 275-278, 10.1103/PhysRev.54.275, 1938.

Niklas, K. J., and Enquist, B. J.: Canonical rules for plant organ biomass partitioning and annual allocation., American Journal of Botany, 89, 812-819, 2002.

Oeser, R. A., Stroncik, N., Moskwa, L.-M., Bernhard, N., Schaller, M., Canessa, R., van den Brink, L., Köster, M., Brucker, E., Stock, S., Fuentes, J. P., Godoy, R., Matus, F. J., Oses Pedraza, R., Osses McIntyre, P., Paulino, L., Seguel, O., Bader, M. Y., Boy, J., Dippold, M. A., Ehlers, T. A., Kühn, P., Kuzyakov, Y., Leinweber, P., Scholten, T., Spielvogel, S., Spohn, M., Übernickel, K., Tielbörger, K., Wagner, D., and von Blanckenburg, F.: Chemistry and Microbiology of the Critical Zone along a steep climate and vegetation gradient in the Chilean Coastal Cordillera., Catena, 170, 183-203, 10.1016/j.catena.2018.06.002, 2018.

Oeser, R. A., and von Blanckenburg, F.: Dataset for evaluation element fluxes released by weathering and taken up by plants along the EarthShape climate and vegetation gradient, GFZ Data Services, 2020.

Pagani, M., Caldeira, K., Berner, R., and Beerling, D. J.: The role of terrestrial plants in limiting atmospheric CO(2) decline over the past 24 million years, Nature, 460, 85-88, 10.1038/nature08133, 2009.

https://doi.org/10.5194/bg-2020-69
Preprint. Discussion started: 9 March 2020

Parada, M. A., and Larrondo, P.: Thermochronology of the Lower Cretaceous Caleu Pluton in the coastal range of central Chile: tectonostratigraphic implications, Abstracts, 4th International Symposium of Andean Geodynamics, Göttingen, 1999, 563-566,

Parada, M. A., Larrondo, P., Guiresse, C., and Roperch, P.: Magmatic Gradients in the Cretaceous Caleu Pluton (Central Chile): Injections of Pulses from a Stratified Magma Reservoir, Gondwana Research, 5, 307-324, 10.1016/s1342-937x(05)70725-5, 2002.

Parada, M. A., López-Escobar, L., Oliveros, V., Fuentes, F., Morata, D., Calderón, M., Aguirre, L., Féraud, G., Espinoza, F., Moreno, H., Figueroa, O., Muñoz Bravo, J., Vásquez, R. T., and Stern, C. R.: Andean magmatism, in: The Geology of Chile, edited by: Moreno, T., and Gibbons, W., The Geological Society of London, 115-146, 2007.

Pearce, C. R., Parkinson, I. J., Gaillardet, J., Chetelat, B., and Burton, K. W.: Characterising the stable (δ 88/86 Sr) and radiogenic (87 Sr/ 86 Sr) isotopic composition of strontium in rainwater, Chemical Geology, 409, 54-60, 10.1016/j.chemgeo.2015.05.010, 2015.

Porada, P., Lenton, T. M., Pohl, A., Weber, B., Mander, L., Donnadieu, Y., Beer, C., Poschl, U., and Kleidon, A.: High potential for weathering and climate effects of non-vascular vegetation in the Late Ordovician, Nat Commun, 7, 12113, 10.1038/ncomms12113, 2016.

Porder, S., Vitousek, P. M., Chadwick, O. A., Chamberlain, C. P., and Hilley, G. E.: Uplift, Erosion, and Phosphorus Limitation in Terrestrial Ecosystems, Ecosystems, 10, 159-171, 10.1007/s10021-006-9011-x, 2007.

Porder, S., and Chadwick, O. A.: Climate and soil-age constraints on nutrient uplift and retention by plants, Ecology, 90, 623-636, 10.1890/07-1739.1, 2009.

Porder, S.: How Plants Enhance Weathering and How Weathering is Important to Plants, Elements, 15, 241-246, 10.2138/gselements.15.4.241, 2019.

Poszwa, A., Dambrine, E., Ferry, B., Pollier, B., and Loubet, M.: Do deep tree roots provide nutrients to the tropical rainforest, Biogeochemistry, 60, 97-118, 2002.

Powers, J. S., Becklund, K. K., Gei, M. G., Iyengar, S. B., Meyer, R., O'Connell, C. S., Schilling, E. M., Smith, C. M., Waring, B. G., and Werden, L. K.: Nutrient addition effects on tropical dry forests: a mini-review from microbial to ecosystem scales, Frontiers in Earth Science, 3, 10.3389/feart.2015.00034, 2015.

Quirk, J., Leake, J. R., Banwart, S. A., Taylor, L. L., and Beerling, D. J.: Weathering by tree-root-associating fungi diminishes under simulated Cenozoic atmospheric CO₂ decline, Biogeosciences, 11, 321-331, 10.5194/bg-11-321-2014, 2014.

Redfield, A. C.: On the proportions of organic derivatives in sea water and their relation to the composition of plankton, James Johnstone memorial volume, 176-192, 1934.

Riebe, C. S., Kirchner, J. W., Granger, D. E., and Finkel, R. C.: Strong tectonic and weak climatic control of long-term chemical weathering rates, Geology, 29, 511-514, 10.1130/0091-7613, 2001.

Riebe, C. S., and Granger, D. E.: Quantifying effects of deep and near-surface chemical erosion on cosmogenic nuclides in soils, saprolite, and sediment, Earth Surface Processes and Landforms, 38, 523-533, 10.1002/esp.3339, 2013.

Rosenstock, N. P.: Can ectomycorrhizal weathering activity respond to host nutrient demands?, Fungal Biology Reviews, 23, 107-114, 10.1016/j.fbr.2009.11.003, 2009.

Rosling, A., Lindahl, B. r. D., Taylor, A. F. S., and Finlay, R. D.: Mycelial growth and substrate acidification of ectomycorrhizal fungi in response to different minerals, FEMS Microbiology Ecology, 47, 31-37, 10.1016/s0168-6496(03)00222-8, 2004.

Rundel, P. W., Ehleringer, J., Mooney, H. A., and Gulmon, S. L.: Patterns of drought response in leaf-succulent shrubs of the coastal Atacama Desert in Northern Chile, Oecologia, 46, 196-200, 10.1007/BF00540126, 1980.

Sardans, J., Rivas-Ubach, A., and Peñuelas, J.: The elemental stoichiometry of aquatic and terrestrial ecosystems and its relationships with organismic lifestyle and ecosystem structure and function: a review and perspectives, Biogeochemistry, 111, 1-39, 10.1007/s10533-011-9640-9, 2011.

Scatena, F. N., and Lugo, A. E.: Geomorphology, disturbance, and the soil and vegetation of two subtropical wet steepland watersheds of Puerto Rico, Geomorphology, 13, 199-213, 10.1016/0169-555x(95)00021-v, 1995.

Schaller, M., Ehlers, T. A., Lang, K. A. H., Schmid, M., and Fuentes-Espoz, J. P.: Addressing the contribution of climate and vegetation cover on hillslope denudation, Chilean Coastal Cordillera (26°–38°S), Earth and Planetary Science Letters, 489, 111-122, 10.1016/j.epsl.2018.02.026, 2018.

Schuessler, J. A., Kämpf, H., Koch, U., and Alawi, M.: Earthquake impact on iron isotope signatures recorded in mineral spring water, Journal of Geophysical Research: Solid Earth, 121, 1-21, 10.1002/2016JB013408, 2016.

Schuessler, J. A., von Blanckenburg, F., Bouchez, J., Uhlig, D., and Hewawasam, T.: Nutrient cycling in a tropical montane rainforest under a supply-limited weathering regime traced by elemental mass balances and Mg stable isotopes, Chemical Geology, 497, 74-87, 10.1016/j.chemgeo.2018.08.024, 2018.

Schwartzmann, D.: The Geobiology of Weathering: a 13th Hypothesis, arXiv preprint arXiv:1509.04234, 2015.

Silver, W. L., and Miya, R. K.: Global patterns in root decomposition: comparisons of climate and litter quality effects, Oecologia, 129, 407-419, 10.1007/s004420100740, 2001.

Spohn, M., and Sierra, C. A.: How long do elements cycle in terrestrial ecosystems?, Biogeochemistry, 139, 69-83, 10.1007/s10533-018-0452-z, 2018.

Sterner, R. W., and Elser, J. J.: Ecological Stoichiometry: The Biology of Elements from Molecules to the Biosphere, 2003.

https://doi.org/10.5194/bg-2020-69
Preprint. Discussion started: 9 March 2020

Stock, S. C., Köster, M., Dippold, M. A., Nájera, F., Matus, F., Merino, C., Boy, J., Spielvogel, S., Gorbushina, A., and Kuzyakov, Y.: Environmental drivers and stoichiometric constraints on enzyme activities in soils from rhizosphere to continental scale, Geoderma, 337, 973-982, 10.1016/j.geoderma.2018.10.030, 2019.

Tessier, A., Campbell, P. G. C., and Bisson, M.: Sequential Extraction Procedure for the Speciation of Particulate Trace Metals, Analytical Chemistry, 51, 844-851, 1979.

Tiessen, H., and Moir, J. O.: Characterization of available P by sequential extraction, in: Soil sampling and methods of analysis, Lewis Publishers Boca Raton, FL, USA, 5-229, 1993.

Uhlig, D., Schuessler, J. A., Bouchez, J. L., Dixon, J., and von Blanckenburg, F.: Quantifying nutrient uptake as driver of rock weathering in forest ecosystems by magnesium stable isotopes, Biogeosciences Discussions, 1-28, 10.5194/bg-2016-521, 2017.

Uhlig, D., and von Blanckenburg, F.: How Slow Rock Weathering Balances Nutrient Loss During Fast Forest Floor Turnover in Montane, Temperate Forest Ecosystems, Frontiers in Earth Science, 7, 10.3389/feart.2019.00159, 2019.

van Dongen, R., Scherler, D., Wittmann, H., and von Blanckenburg, F.: Cosmogenic 10Be in river sediment: where grain size matters and why, Earth Surface Dynamics, 7, 393-410, 10.5194/esurf-7-393-2019, 2019.

van Schöll, L., Kuyper, T. W., Smits, M. M., Landeweert, R., Hoffland, E., and Breemen, N. v.: Rock-eating mycorrhizas: their role in plant nutrition and biogeochemical cycles, Plant and Soil, 303, 35-47, 10.1007/s11104-007-9513-0, 2007.

Vitousek, P. M., Hedin, L. O., Matson, P. A., Fownes, J. H., and Neff, J.: Within-System Element Cycles, Input-Output Budgets, and Nutrient Limitation, in: Successes, Limitations, and Frontiers in Ecosystem Science, Springer, New York, 432-451, 1998.

Vitousek, P. M.: Nutrient Cycling and Limitation: Hawai'i as a Model System, PRINCETON ENVIRONMENT AL INSTITUTE SERIES, 2004.

Vitousek, P. M., Porder, S., Houlton, B. Z., and Chadwick, O. A.: Terrestrial phosphorus limitation: mechanisms, implications, and nitrogen–phosphorus interactions, Ecological Applications, 20, 5-15, 10.1890/08-0127.1, 2010.

von Blanckenburg, F., Wittmann, H., and Schuessler, J. A.: HELGES: Helmholtz Laboratory for the Geochemistry of the Earth Surface, Journal of large-scale research facilities JLSRF, 2, 10.17815/jlsrf-2-141, 2016.

Wang, F., Michalski, G., Seo, J.-h., and Ge, W.: Geochemical, isotopic, and mineralogical constraints on atmospheric deposition in the hyper-arid Atacama Desert, Chile, Geochimica et Cosmochimica Acta, 135, 29-48, 10.1016/j.gca.2014.03.017, 2014.

Werner, C., Schmid, M., Ehlers, T. A., Fuentes-Espoz, J. P., Steinkamp, J., Forrest, M., Liakka, J., Maldonado, A., and Hickler, T.: Effect of changing vegetation and precipitation on denudation – Part 1: Predicted vegetation composition and cover over the last 21 thousand years along the Coastal Cordillera of Chile, Earth Surface Dynamics, 6, 829-858, 10.5194/esurf-6-829-2018, 2018.

White, A. E., Spitz, Y. H., Karl, D. M., and Letelier, R. M.: Flexible elemental stoichiometry in Trichodesmium spp. and its ecological implications, Limnology and Oceanography, 51, 1777-1790, 10.4319/lo.2006.51.4.1777, 2006.

White, A. F., Blum, A. E., Schulz, M. S., Vivit, D. V., Stonestrom, D. A., Larsen, M., Murphy, S. F., and Eberl, D.: Chemical Weathering in a Tropical Watershed, Luquillo Mountains, Puerto Rico: I. Long-Term Versus Short-Term Weathering Fluxes, Geochimica et Cosmochimica Acta, 62, 209-226, 10.1016/s0016-7037(97)00335-9, 1998.

Wilcke, W., Yasin, S., Abramowski, U., Valarezo, C., and Zech, W.: Nutrient storage and turnover in organic layers under tropical montane rain forest in Ecuador, European Journal of Soil Science, 53, 15-27, 2002.

Wilcke, W., Velescu, A., Leimer, S., Bigalke, M., Boy, J., and Valarezo, C.: Biological versus geochemical control and environmental change drivers of the base metal budgets of a tropical montane forest in Ecuador during 15 years, Biogeochemistry, 136, 167-189, 10.1007/s10533-017-0386-x, 2017.

Winnick, M. J., and Maher, K.: Relationships between CO2, thermodynamic limits on silicate weathering, and the strength of the silicate weathering feedback, Earth and Planetary Science Letters, 485, 111-120, 10.1016/j.epsl.2018.01.005, 2018.

https://doi.org/10.5194/bg-2020-69
Preprint. Discussion started: 9 March 2020

Biogeosciences
Discussions
Open Access
EGU

14 Figures

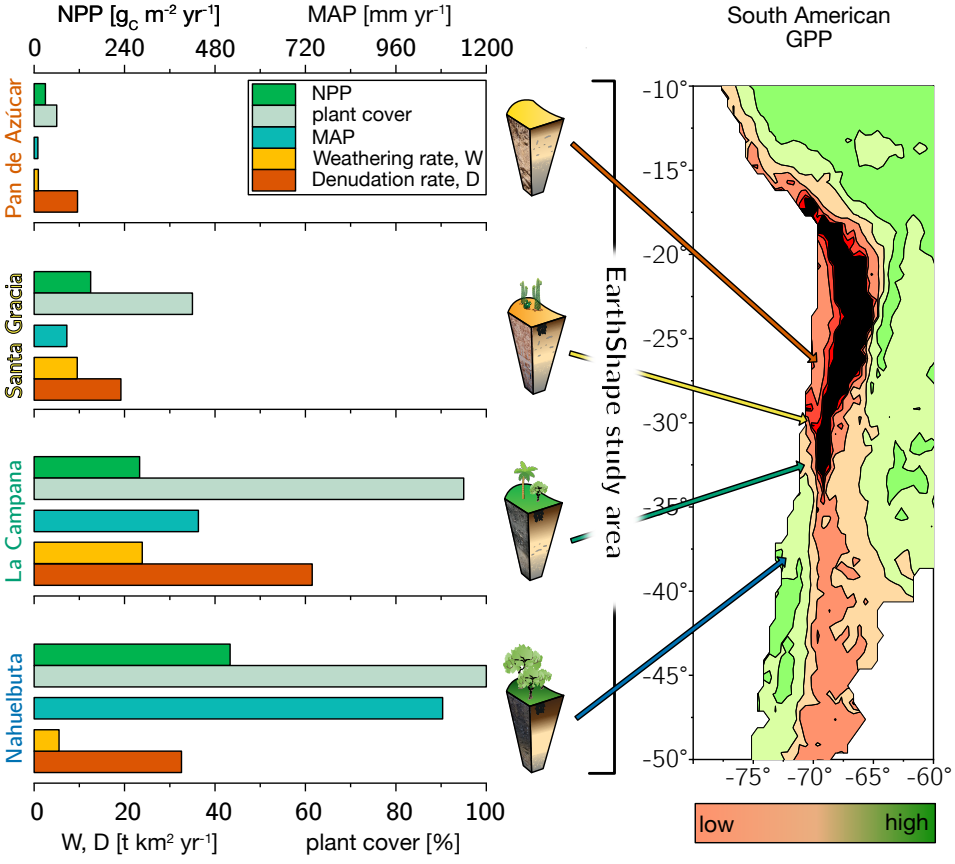

Figure 1 The climate and vegetation gradient of the four EarthShape study sites (from arid to humid: Pan de Azúcar, Santa Gracia, La Campana, and Nahuelbuta). Left: Net primary productivity (NPP), plant cover, annual precipitation (MAP). Denudation rate (D) and weathering rate (W) were determined with cosmogenic ^{10}Be. Right: Position of the four study sites in South America and their respective gross primary productivity (GPP) derived from the FLUXNET data base (Jung et al., 2011). Black colour refers to very low GPP in the Atacama Desert.

https://doi.org/10.5194/bg-2020-69
Preprint. Discussion started: 9 March 2020

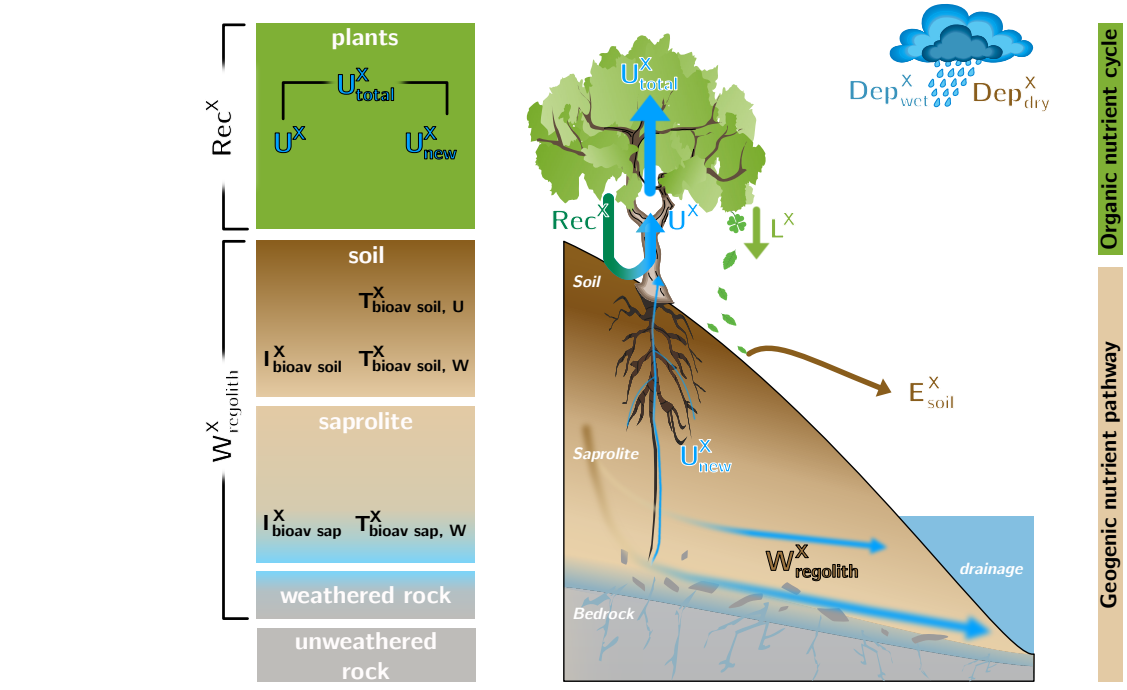

Figure 2 Conceptual framework of an ecosystem comprising the "geogenic nutrient pathway" and the "organic nutrient cycle" (modified after Uhlig and von Blanckenburg, 2019). Whereas the former is mainly set by mineral nutrient release by weathering ($W^X_{regolith}$) and to a minor extent by atmospheric wet- (Dep^X_{wet}) and dry deposition (Dep^X_{dry}), the organic nutrient cycle is mainly affected by nutrient re-utilization (i.e. recycling) from organic matter (Rec^X). Left: The different compartments (i.e. rock, saprolite, soil, the litter layer, and biota) are shown as boxes. They include the metrics used to quantify their properties such as the inventory I^X_{bulk} and turnover time $T^X_{i,j}$ of element X in compartment j. Right: The compartments are linked by fluxes (arrows) with the thickness of them denoting to their relative proportions. E^X_{soil} denotes to erosion of soil.

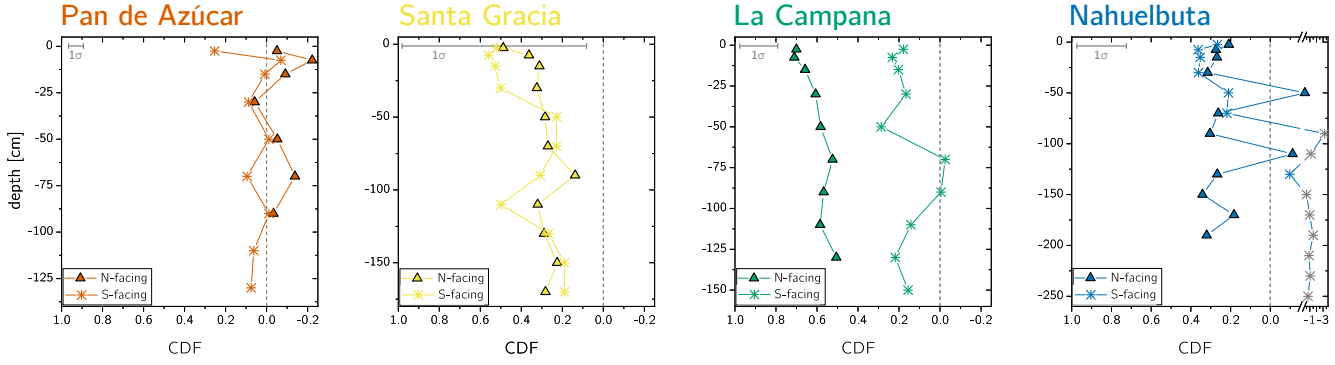

Figure 3 Chemical depletion fraction (CDF) for each study sites' north- and south- facing profile. The accuracy of the absolute CDF values is limited by the variability in the bedrocks' Zr concentration in the respective study sites and are indicated as grey 1 σ bar (Table S1). The grey symbols correspond mainly to saprolite samples in the south-facing regolith profile in Nahuelbuta and are excluded from further consideration. Note that in Nahuelbuta a different scaling compared to the other study sites applies after the axis break.

https://doi.org/10.5194/bg-2020-69
Preprint. Discussion started: 9 March 2020

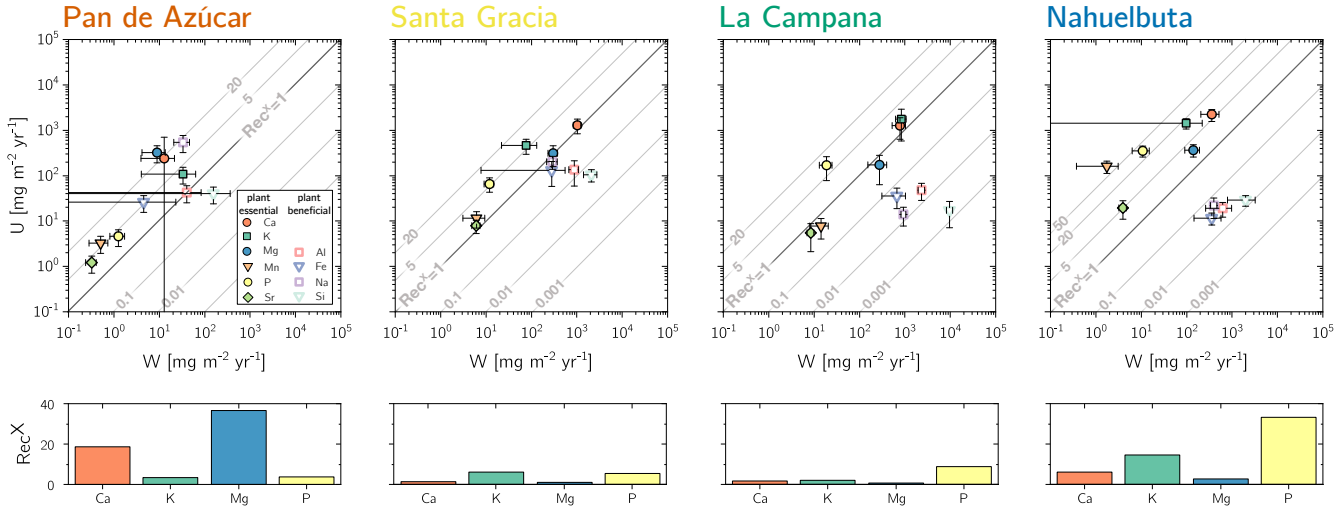

Figure 4 Chemical weathering flux ($W^X_{regolith}$) and plant nutrient-uptake fluxes (U^X_{total}) for Pan de Azúcar, Santa Gracia, La Campana, and Nahuelbuta (from left to right) for plant-essential and plant-beneficial elements. Grey contour lines emphazize the nutrient recycling factor (Rec^X), which is the ratio of U^X_{total} to $W^X_{regolith}$. Uncertainty bars show 1SD. Differences in nutrient recycling factors for the plant essential elements Ca, K, Mg, and P among the four study sites are highlighted in the lower panels. Note that here we use the Rec^X calculated for $W^X_{regolith}$ from silicate weathering only. In Table 7 and Fig. A4 we also show Rec^X including atmospheric inputs. Because Pan de Azúcar Ca and Mg inputs are exclusively atmospheric their Rec^X are overestimated and thus not plotted on the lower left panel.

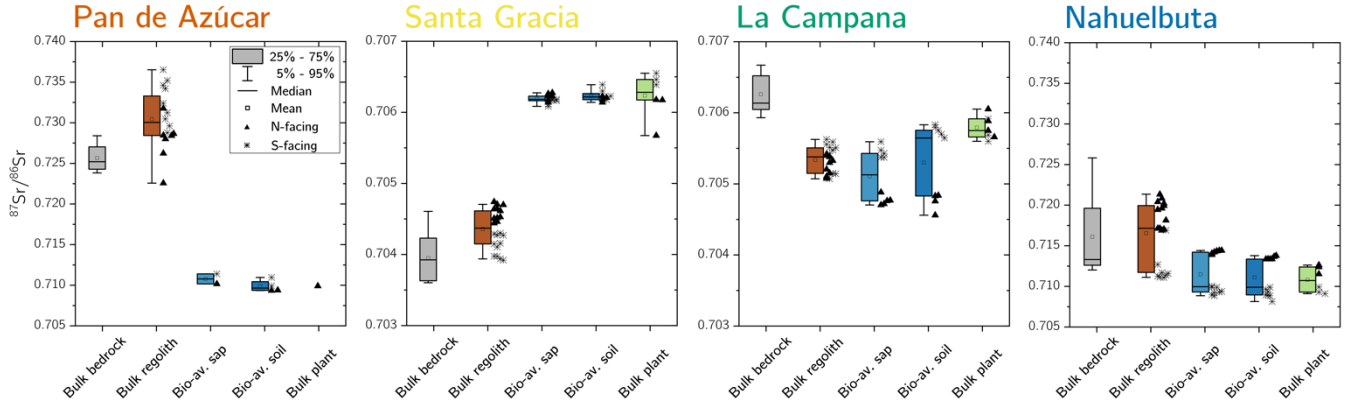

Figure 5 Average $^{87}Sr/^{86}Sr$ isotope composition of bedrock, bulk regolith, and the bio-available fraction in saprolite, soil, and plants in Pan de Azúcar, Santa Gracia, La Campana, and Nahuelbuta. The $^{87}Sr/^{86}Sr$ isotope ratios of bulk plant (green) are weighted according to the single species' organs relative growth rate (see Table 5 for weighting parameters). Whiskers span 90% of the respective data set. On the boxes' right-hand site, the differences between north- and south-facing regolith profiles are depicted. Note that bulk regolith samples in Nahuelbuta with anomalously low Zr concentrations have been excluded from this analysis as they are suspected to comprise a different parent rock. Y-axis covers broader range in Pan de Azúcar and Nahuelbuta than Santa Gracia and La Campana.

https://doi.org/10.5194/bg-2020-69
Preprint. Discussion started: 9 March 2020

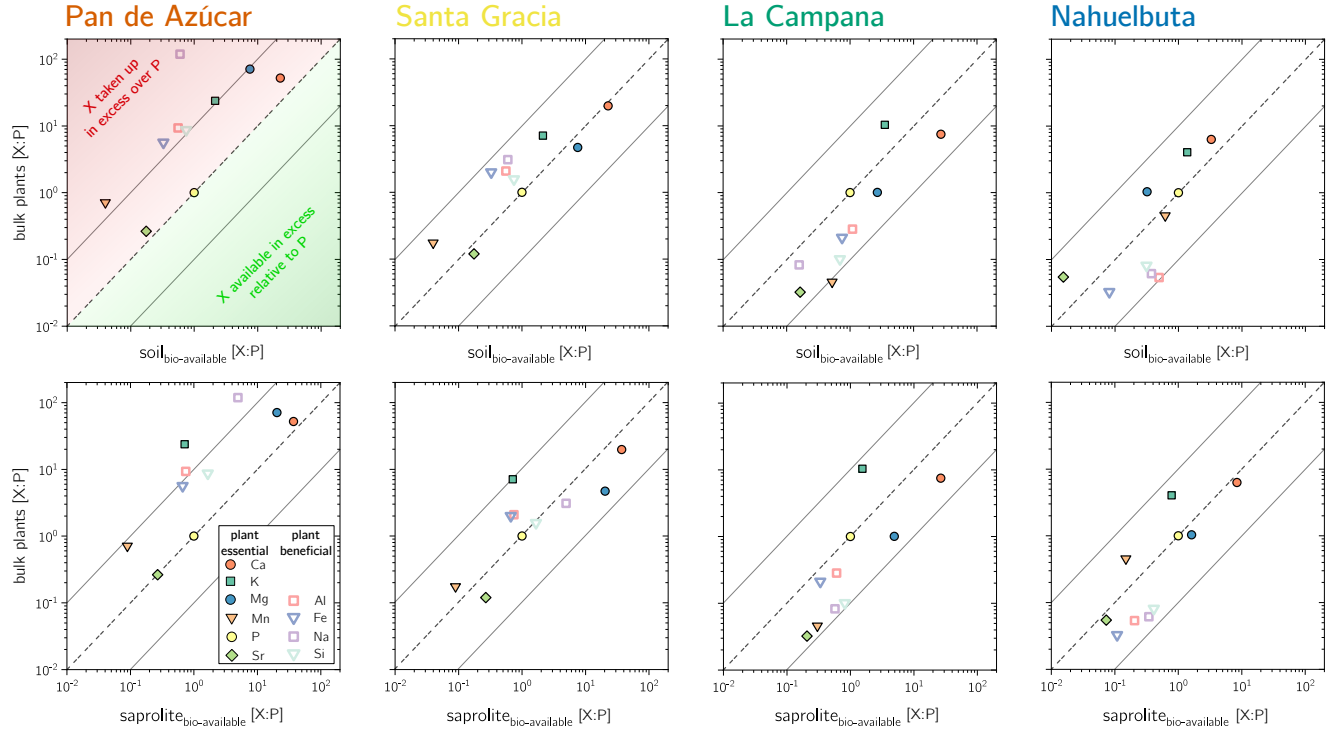

Figure 6 P-normalized element composition for bulk plants and the bio-available fraction in soil and saprolite in Pan de Azúcar, Santa Gracia, La Campana, and Nahuelbuta. Solid grey lines reflect the 10- and 0.1-fold P concentration, respectively. Elements from within this envelope are believed to set the ecosystems' ecological stoichiometry. Elements above the dashed grey line are taken up in excess over P, below the line they exist in surplus in the bio-available soil fraction.

https://doi.org/10.5194/bg-2020-69
Preprint. Discussion started: 9 March 2020

Biogeosciences Discussions Open Access EGU

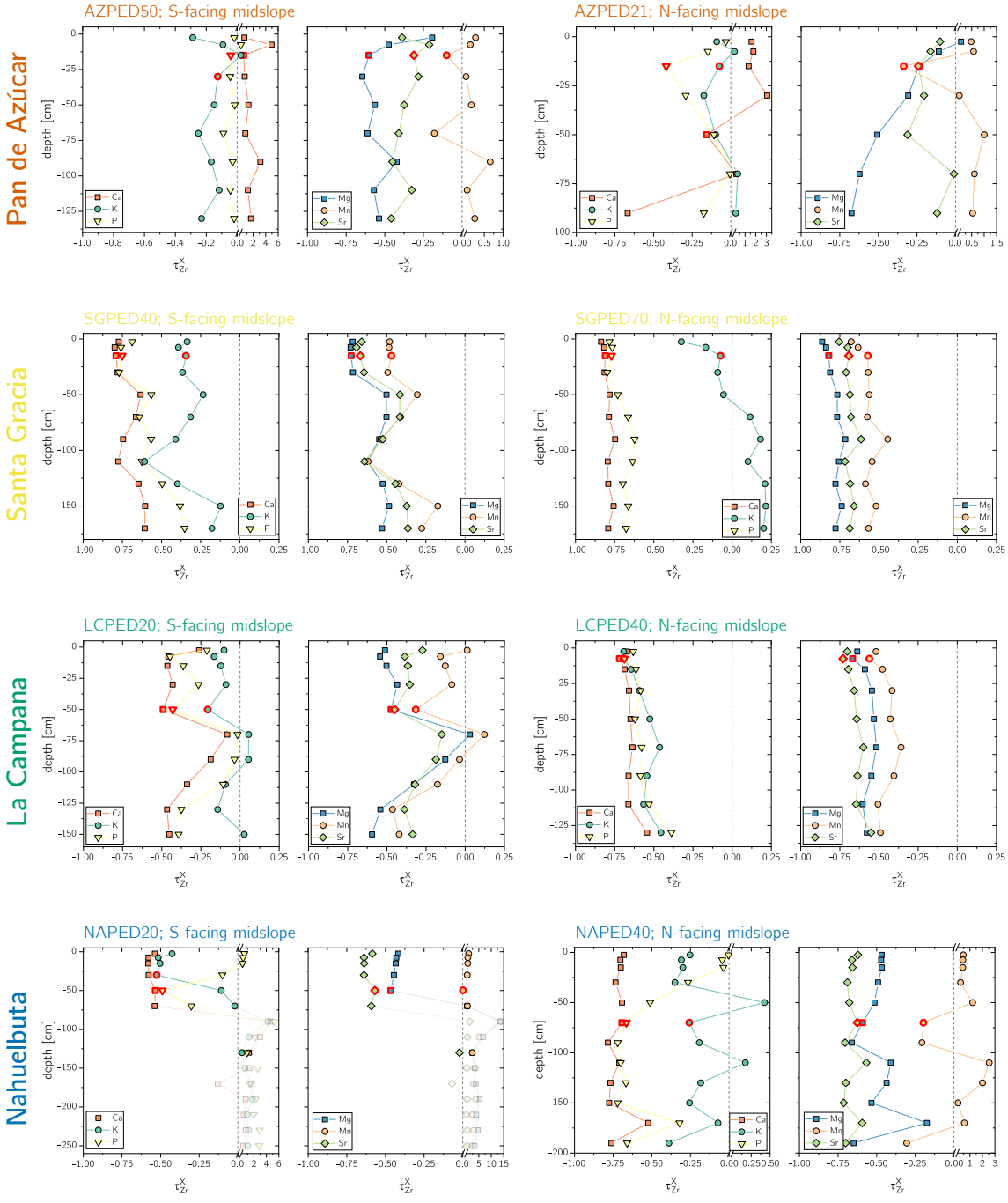

Figure A1. Depth distribution of the elemental loss and gain fractions (i.e. elemental mass transfer coefficient, τ) for Pan de Azúcar, Santa Gracia, La Campana, and Nahuelbuta. The vertical dashed line indicates $\tau_{Zr}^{X} = 0$ and represents unweathered parent bedrock. τ-values corresponding to the shallowest mineral soil samples are highlighted with a red rim. Grey symbols in Nahuelbuta are discarded due to the samples' anomalous low Zr concentration. Note that these τ-values deviate from those reported in Oeser et al., 2018, such that in this work they have been calculated relative to the bedrocks' initial chemical composition.

https://doi.org/10.5194/bg-2020-69
Preprint. Discussion started: 9 March 2020

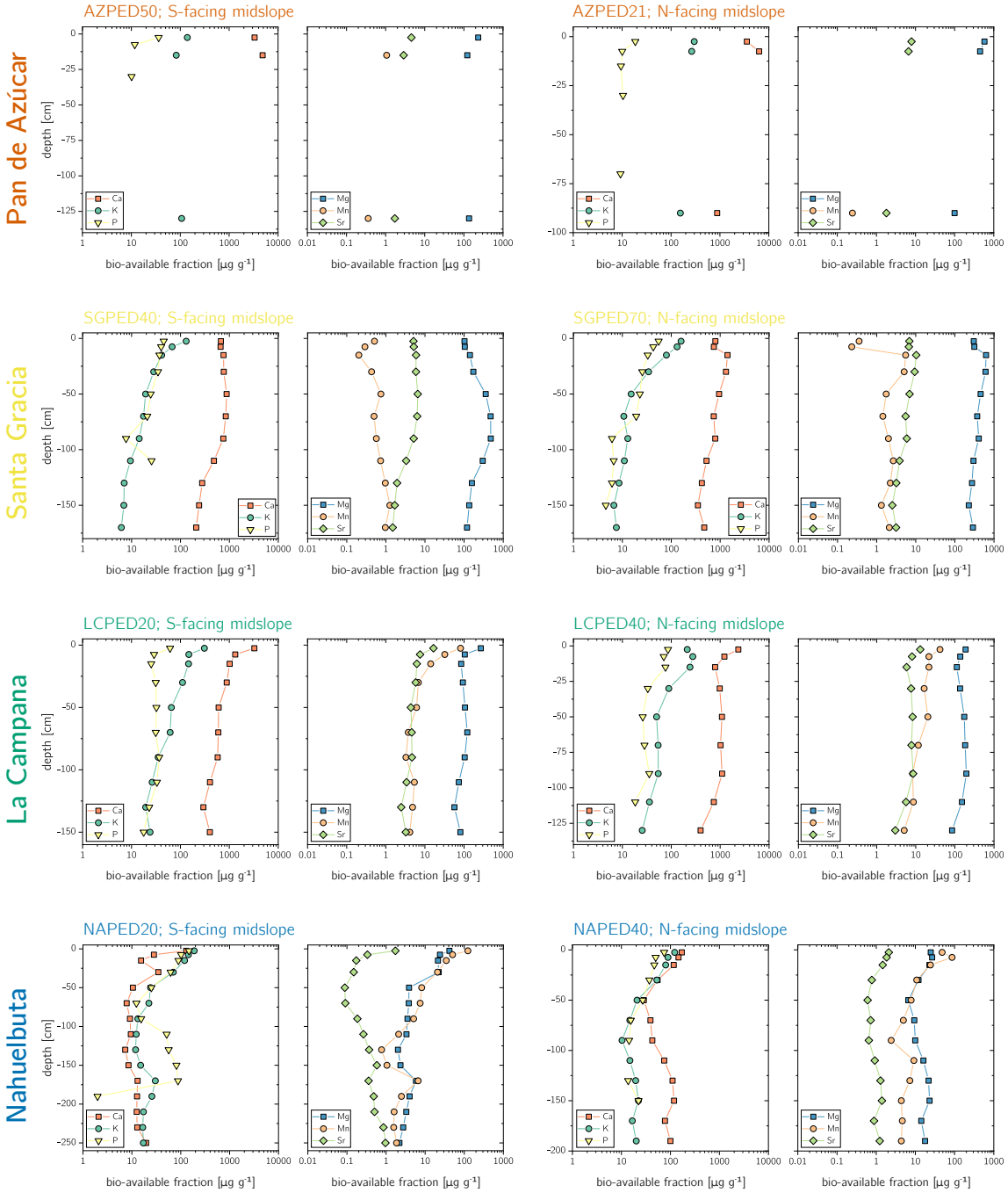

Figure A2. Depth distribution of the concentration of sequentially extracted bio-available fraction of plant-essential elements including Sr, comprised of the water soluble (18 MΩ Milli-Q H_2O) and the exchangeable (1 M NH_4OAc) fraction at Pan de Azúcar, Santa Gracia, La Campana, and Nahuelbuta. Note that in Pan de Azúcar the acquisition of the bio-available fraction was only possible on three samples per site. Data gaps do occur if both extractions of one sample were below limit of detection.

https://doi.org/10.5194/bg-2020-69
Preprint. Discussion started: 9 March 2020

Biogeosciences Discussions Open Access EGU

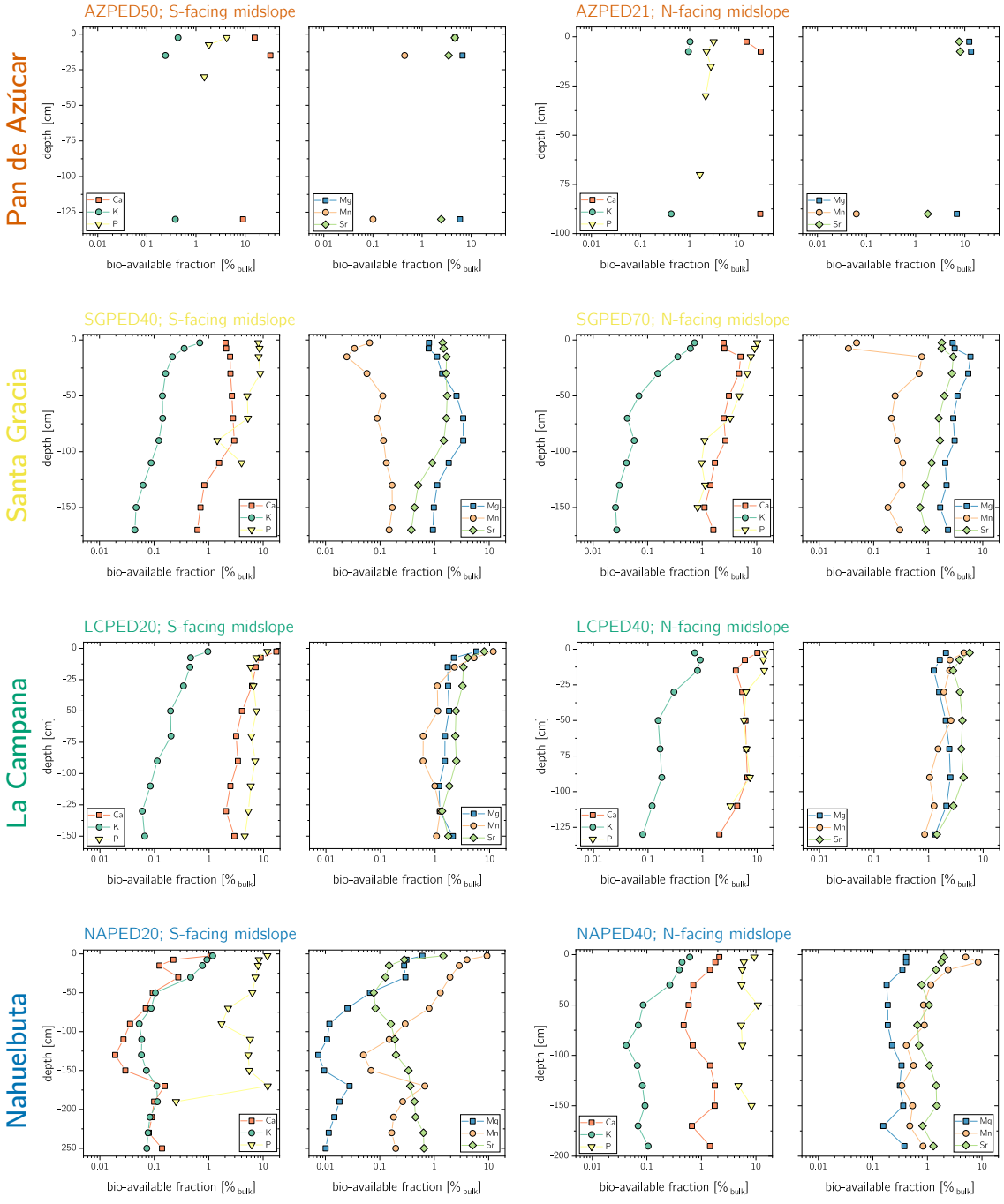

Figure A3. Depth distribution of the sequentially extracted bio-available fraction of plant-essential elements relative to their respective amount contained in bulk regolith including Sr, comprised of the water soluble (18 MΩ Milli-Q H_2O) and the exchangeable (1 M NH_4OAc) fraction samples at Pan de Azúcar, Santa Gracia, La Campana, and Nahuelbuta. Note that in Pan de Azúcar the acquisition of the bio-available fraction was only possible on three samples per site. Data gaps do occur if both extractions of one sample were below limit of detection.

https://doi.org/10.5194/bg-2020-69
Preprint. Discussion started: 9 March 2020

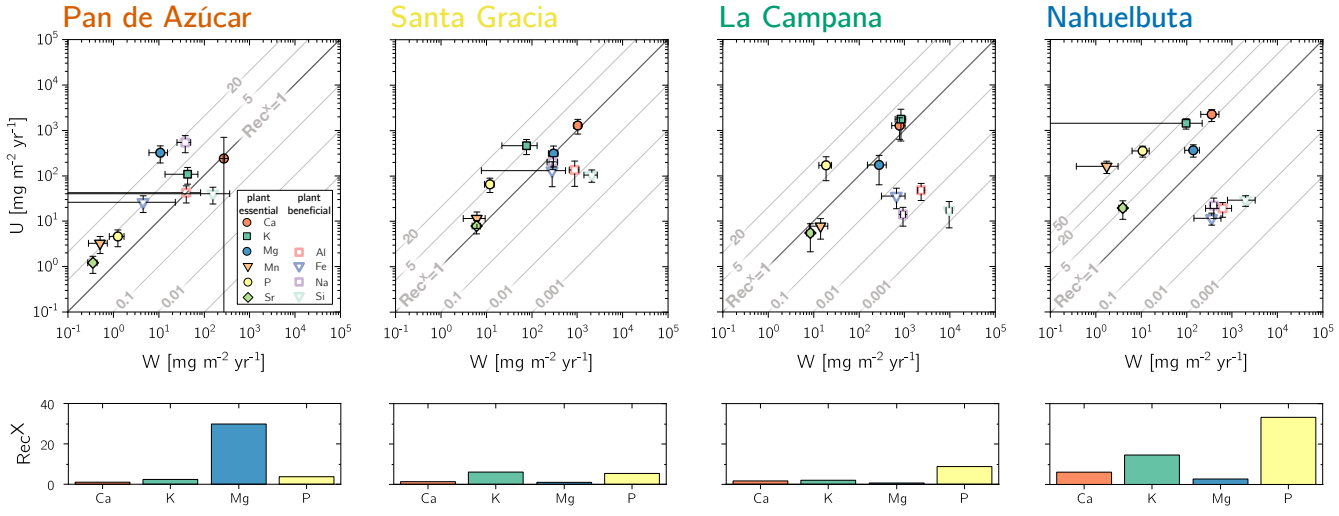

Figure A4. Chemical weathering flux ($W^X_{regolith}$) and ecosystem nutrient-uptake fluxes (U^X_{total}) for Pan de Azúcar, Santa Gracia, La Campana, and Nahuelbuta (from left to right) for plant-essential (closed symbols) and plant-beneficial elements (open symbols). Weathering-release fluxes for Ca, K, Mg, Na, and Sr in Pan de Azúcar have been complemented by atmospheric depositional fluxes such that the total amount of available nutrients increase by 95, 22, 18, 12, and 10%, respectively. Grey contour lines emphasize the nutrient recycling factor (Rec^X), which is the ratio of U^X_{total} to $W^X_{regolith}$. Uncertainty bars show 1SD. Differences in nutrient recycling factors for the plant essential elements Ca, K, Mg, and P among the four study sites are highlighted in the lower panels.

15 Tables

https://doi.org/10.5194/bg-2020-69
Preprint. Discussion started: 9 March 2020

Table 1 Characteristics of the four EarthShape study sites and soil profile names in Pan de Azúcar, Santa Gracia, La Campana, and Nahuelbuta.

		Pan de Azúcar		Santa Gracia		La Campana		Nahuelbua		
		AZPED21	*AZPED50*	*SGPED70*	*SGPED40*	*LCPED40*	*LCPED20*	*NAPED40*	*NAPED20*	*Reference*
Latitude		26.1093 S	26.1102 S	29.7612 S	29.7574 S	32.9573 S	32.9559 S	37.8090 S	37.8077 S	†
Longitude		70.5491 W	70.5493 W	71.1656 W	71.1664 W	71.0643 W	71.0635 W	73.0138 W	73.0135 W	†
Altitude	[m a.s.l.]	343	330	690	682	734	730	1219	1239	*
Slope	[°]	25	40	15	25	12	23	13	15	‡
Aspect		N-facing	S-facing	N-facing	S-facing	N-facing	S-facing	N-facing	S-facing	†, ‡
Mean annual temperature (MAT)	[°C]	18.1		16.1		14.9		14.1		§
Mean annual precipitation (MAP)	[mm yr^{-1}]	10		87		436		1084		§
Lithology		granite		diorite		granodiorite		granodiorite		†
Mineralogy*	[Vol%]	Quartz xxx, Plagioclase x, K-feldspar xxx, Pyroxene -, Biotite x, Amphibole -		Quartz x, Plagioclase xx, K-feldspar xxx, Pyroxene xx, Biotite -, Amphibole x		Quartz xx, Plagioclase x, K-feldspar xxx, Pyroxene -, Biotite x, Amphibole -		Quartz xx, Plagioclase xx, K-feldspar xxx, Pyroxene x, Biotite x, Amphibole -		†
Soil type		Regosol	Regosol	Cambisol	Leptosol	Cambisol	Cambisol	umbric Podzol	orthodystric Umbrisol	‡
Soil thickness	[cm]	20	20	35	45	35	60	60	70	†
Soil pH**		8.1 ± 0.1	8.1 ± 0.1	6.0 ± 0.3	6.1 ± 0.3	5.2 ± 0.3	5.0 ± 0.3	4.7 ± 0.1	4.3 ± 0.2	‡
Cation exchange capacity (CEC)**	[µmolc g^{-1}]	-	-	108.5 ± 50.2	64.6 ± 23.4	86.4 ± 43.1	72.7 ± 62.1	21.0 ± 15.4	38.2 ± 24.7	‡
Catchment-wide denudation rate (D)	[t km^{-2} yr^{-1}]	7.7 ± 0.7		9.2 ± 0.8		200 ± 22		27.2 ± 2.4		‖
Soil denudation rate (D_{soil})	[t km^{-2} yr^{-1}]	8.2 ± 0.5	11.0 ± 0.7	15.9 ± 0.9	22.4 ± 1.5	69.2 ± 4.6	53.7 ± 3.4	17.7 ± 1.1	47.5 ± 3.0	†, #
Soil weathering rate (W)	[t km^{-2} yr^{-1}]	-1.0 ± 0.1***	0.9 ± 0.2	7.2 ± 4.7	11.9 ± 7.6	45.9 ± 8.0	20.0 ± 3.1	3.5 ± 0.9	7.5 ± 3.1	†, #
Soil erosion rate (E)	[t km^{-2} yr^{-1}]	9.1 ± 0.5	10.1 ± 0.7	8.7 ± 4.8	10.5 ± 7.7	23.4 ± 9.2	33.8 ± 4.6	14.2 ± 1.4	40.0 ± 4.3	†, #
Chemical depletion fraction (CDF)		-0.1 ± 0.0	0.1 ± 0.0	0.5 ± 0.3	0.5 ± 0.3	0.7 ± 0.1	0.4 ± 0.1	0.2 ± 0.1	0.2 ± 0.1	†, #
Vegetation cover	[%]	<5		30 – 40		95		100		‡
Vegetation types		*Cristaria integerrima*, *Nolana mollis*, *Perityle* sp., *Stipa plumosa*, *Tetragonia maritima*		*Adesmia* sp., *Cordia decandra*, *Cumulopuntia sphaerica*, *Eulychnia acida*, *Proustia cuneifolia*, *Senna cumingii*		*Aristeguietia salvia*, *Colliguaja odorifera*, *Cryptocarya alba*, *Jubaea chilensis*, *Lithraea caustica*		*Araucaria araucana*, *Chusquea culeou*, *Nothofagus antarctica*		‡
Net primary production (NPP)	[g_C m^{-2} yr^{-1}]	30 ± 10		150 ± 40		280 ± 50		520 ± 130		¶

* Estimation of mineral abundances based on thin section microscopy: -: absence, x: presence (<10 Vol%), xx: abundant (10-35 Vol%), xxx: very abundant (>35 Vol%)

** Denoting to regolith-profile averages

*** N-facing slope in Pan de Azúcar yield negative CDF and hence weathering rates due to the input of seaspray

† Oeser et al. (2018); ‡ Bernhard et al. (2018); § Ministerio de Obras Públicas (2017); ‖ van Dongen et al. (2019); # Schaller et al. (2018); ¶ Werner et al. (2018)

Biogeosciences Discussions
Open Access
EGU

https://doi.org/10.5194/bg-2020-69
Preprint. Discussion started: 9 March 2020

Biogeosciences Discussions Open Access EGU

Table 2 Glossary of metrics for the parameterization of the geogenic nutrient pathway and organic nutrient cycle in terrestrial ecosystems after Uhlig and von Blanckenburg (2019).

Total mass fluxes (in e.g. t km^{-2} yr^{-1})		
Eq. (1)	$D = E + W$	denudation rate; the sum of chemical weathering and physical erosion
	E	physical erosion; physical removal of primary and secondary minerals along with biogenic material
Eq. (2)	$W = D \times CDF$	chemical weathering rate; net-chemical release flux from minerals as some fraction of which is being incorporated into secondary minerals and pedogenic (hydr-)oxides
	GPP	gross primary production; gross carbon input into biomass
	NPP	net primary productivity; net-carbon fixation by biomass
Elemental fluxes (in e.g. mg m^2 yr^{-1})		
Eq. (3)	$W^X_{regolith} = D \times [X]_{parent} \times (-\tau^X_{Xi})$	Chemical weathering flux of element X; release flux of X from minerals minus the flux of incorporation of X into secondary minerals and oxides
Eq. (4)	$U^X_{total} = \frac{NPP \times [X]_{plant}}{[C]_{plant}}$	Total nutrient uptake flux of element X; uptake of X by trees at the ecosystem scale, where $[C]_{plant}$ denotes the carbon concentration in dry mass, typically 50 weight%
	Dep^X_{dry}	Atmospheric dry deposition of element X
	Dep^X_{wet}	Atmospheric wet deposition of element X as rainfall
Elemental mass fractions and flux ratios (dimensionless)		
Eq. (5)	$CDF = 1 - \frac{[X_i]_{parent}}{[X_i]_{weathered}}$	chemical depletion fraction; fractional mass loss by dissolution of elements from the regolith
Eq. (6)	$\tau_X = \frac{[X]_{weathered}}{[X]_{parent}} \times \frac{[X_i]_{parent}}{[X_i]_{weathered}} - 1$	elemental mass transfer coefficient; elemental loss or gain relative to unweathered bedrock
Eq. (7)	$Rec^X = \frac{U^X_{total}}{W^X_{regolith}}$	nutrient recycling factor; number of times, element X is re-utilized from plant litter after its initial release from rock weathering
Elemental inventories (in e.g. g m^{-2} or kg m^{-2})		
Eq. (8)	$I_j = \int_{z=a}^{z=b} [X_j] \times \rho \, dz$	Inventory of element X in compartment j
	$I^X_{bio\text{-}av.\ soil}$	Inventory of element X in the bio-available fraction in soil
	$I^X_{bio\text{-}av.\ sap}$	Inventory of element X in the bio-available fraction in saprolite
	I^X_{bulk}	Inventory of element X in bulk regolith
Elemental turnover times (in e.g. yr)		
Eq. (9)	$T^X_{i,j} = \frac{I^X_i}{j}$	Turnover time of element X in compartment i with respect to input or output flux j; the ratio of total stock of element X in i to input or output flux j
	$T^X_{bio\text{-}av,\ U}$	Turnover time of element X in the forest floor with respect to uptake into trees; mean time a nutrient rest in the forest floor before re-utilization by forest trees
	$T^X_{bio\text{-}av,\ W}$	Turnover time of element X in the bio-available fraction in regolith with respect to adsorption onto clay minerals; mean time over which the inventory of the bio-available fraction is replenished by chemical silicate weathering in the absence of other gains or losses

https://doi.org/10.5194/bg-2020-69
Preprint. Discussion started: 9 March 2020

Biogeosciences Discussions Open Access EGU

1080 **Table 3 Elemental weathering fluxes ($W^X_{regolith}$) and ecosystem nutrient uptake fluxes (U^X_{total}) in Pan de Azúcar, Santa Gracia, La Campana, and Nahuelbuta along with the respective study site's average denudation rate (D) and net primary productivity (NPP).**

Study site	D [t km^{-2} yr^{-1}]	NPP [g$_C$ m^{-2} yr^{-1}]	Al	Ca	Fe	K	Mg	Mn	Na	P	Si	Sr
			[mg m^{-2} yr^{-1}]									
Pan de Azúcar												
$W^X_{regolith}$	9.6		40	13*	5	30	9	0.5	33	1.3	160	0.3
SD	*0.6*		*43*	*9*	*18*	*30*	*5*	*0.2*	*13*	*0.4*	*210*	*0.1*
U^X_{total}	-	30	40	200	30	110	300	3	500	5	40	1.2
SD	-	*10*	*20*	*500*	*10*	*40*	*100*	*1*	*200*	*2*	*20*	*0.5*
Santa Gracia												
$W^X_{regolith}$	19.2		870	1030	280	80	300	6	290	12	2100	6.1
SD	*1.2*		*200*	*200*	*270*	*50*	*70*	*3*	*80*	*3*	*680*	*1.3*
U^X_{total}	-	150	140	1300	130	500	300	12	200	70	100	8
SD	-	*40*	*80*	*500*	*70*	*200*	*100*	*5*	*60*	*20*	*30*	*3*
La Campana												
$W^X_{regolith}$	61.5		2330	770	670	840	280	14	930	19	9700	8.5
SD	*4.0*		*370*	*250*	*350*	*220*	*120*	*6*	*110*	*6*	*1500*	*1.5*
U^X_{total}	-	280	50	1300	40	2000	200	8	14	170	17	6
SD	-	*50*	*20*	*600*	*20*	*1000*	*100*	*4*	*6*	*90*	*10*	*3*
Nahuelbuta												
$W^X_{regolith}$	32.6		620	360	360	100	140	1	400	11	2000	4.0
SD	*2.1*		*360*	*150*	*210*	*120*	*50*	*3*	*70*	*4*	*1200*	*0.7*
U^X_{total}	-	520	19	2200	12	1400	400	160	22	350	30	19
SD	-	*130*	*7*	*700*	*3*	*400*	*100*	*50*	*11*	*100*	*10*	*9*

* $W^X_{regolith}$ only includes information from AZPED21 (N-facing slope regolith profile) as atmospheric deposition of Ca in the S-facing slope led to (theoretically) negative weathering fluxes.

Uncertainties on weathering fluxes are estimated by Monte-Carlo simulations, where the SD of the respective profile's denudation rate, the SD of the bedrocks' element concentration of interest, and 3% relative uncertainty on the element concentration in regolith samples have been used.

Uncertainties on nutrient uptake fluxes are estimated by Monte-Carlo simulations, where the SD of the respective study site's net primary productivity (NPP) and the SD of the chemical composition of the weighted above-ground living ecosystem have been used (Table 5)

https://doi.org/10.5194/bg-2020-69
Preprint. Discussion started: 9 March 2020

Biogeosciences Discussions Open Access EGU

Table 4 Inventories of plant-essential and plant-beneficial elements in bulk regolith and the bio-available fraction in soil and saprolite. Apart from phosphorus, the accessibility of these elements was determined using a sequential extraction method described by Arunachalam et al. (1996); Tessier et al. (1979); He et al. (1995). P-accessibility in the bio-available fraction has been determined by Brucker and Spohn (2019) using a modified Hedley sequential P fractionation method. Supplementary Tables S3 & S4 include depth-dependent concentration of the bio-available fraction (pooled) and the Milli-Q and NH4OAc extractions used for calculation of the inventories (Oeser and von Blanckenburg, 2020).

Study site		Extent* [m]	Al	Ca	Fe	K	Mg	Mn	Na	P	Si	Sr	Σ
Pan de Azúcar													
$I^{X}_{bio\text{-}av,\ soil}$	[g m^{-2}]	0.2	0.3	1440	n.c.	53	92	0.1	493	3.3	19	1.5	2100
$I^{X}_{bio\text{-}av,\ sap}$	[g m^{-2}]	1.0	1.7	3833	n.c.	253	244	0.6	682	0.0	75	3.5	5100
I^{X}_{bulk}	[kg m^{-2}]	1.0	136	21	44	65	8.6	0.5	39	1.3	636	0.2	950
Santa Gracia													
$I^{X}_{bio\text{-}av,\ soil}$	[g m^{-2}]	0.4	12	616	7.2	38	221	1.4	18	22	19	4.6	960
$I^{X}_{bio\text{-}av,\ sap}$	[g m^{-2}]	1.0	23	1179	21	23	651	2.9	159	21	53	8.5	2100
I^{X}_{bulk}	[kg m^{-2}]	1.0	183	130	75	29	42	1.5	61	1.6	532	1.0	1100
La Campana													
$I^{X}_{bio\text{-}av,\ soil}$	[g m^{-2}]	0.5	37	673	24	90	79	11	6.7	28	34	4.5	1000
$I^{X}_{bio\text{-}av,\ sap}$	[g m^{-2}]	1.0	51	1026	23	70	191	12	31	39	142	8.0	1600
I^{X}_{bulk}	[kg m^{-2}]	1.0	118	26	49	46	10	0.9	31	0.7	456	0.3	740
Nahuelbuta													
$I^{X}_{bio\text{-}av,\ soil}$	[g m^{-2}]	0.9	14	60	1.8	39	9.9	15	17	31	14	0.5	200
$I^{X}_{bio\text{-}av,\ sap}$	[g m^{-2}]	1.0	1.5	52	< 0.5	19	11	3.9	13	23	12	0.8	140
I^{X}_{bulk}	[kg m^{-2}]	1.0	95	15	47	22	13	1.0	10	0.7	309	0.1	510

$I^{X}_{bio\text{-}av,\ soil}$ = inventory of element X in the soil bio-available fraction; extent amounts to maximum soil depth

$I^{X}_{bio\text{-}av,\ sap}$ = inventory of element X in the saprolite bio-available fraction;

I^{X}_{bulk} = inventory of element X in bulk regolith

* the extent of the saprolite and regolith inventory have been scaled to 1.0 m for purposes of comparisons between the four study sites and the lack of an absolute measure of the depth of saprolite.

n.c. = not calculated as the respective bio-available fraction (Table S4) was below the limit of calibration of ICP-OES measurements

https://doi.org/10.5194/bg-2020-69
Preprint. Discussion started: 9 March 2020

Biogeosciences Discussions Open Access EGU

Table 5 Chemical composition of the above ground living plants. Plant organs have been weighted according to Niklas and Enquist (2002), using the plant organs' relative growth rate (see Appendix A). Relative growth rates and relative abundance of the different plant species can be found in this table's footnotes. The unweighted chemical composition of each plant organ is listed in Table S5 (Oeser and von Blanckenburg, 2020).

Study site	Al	Ca	Fe	K	Mg	Mn	Na	P	Si	Sr
					[µg g^{-1}]					
Pan de Azúcar†										
mean	2700	15200	1700	6900	20700	210	34600	290	2500	80
SD	*300*	*1500*	*200*	*700*	*2100*	*20*	*3500*	*30*	*300*	*10*
Santa Gracia‡										
mean	1880	17800	1800	6400	4200	160	2800	900	1400	110
SD	*920*	*4400*	*900*	*1600*	*1700*	*50*	*500*	*220*	*300*	*20*
SE (n=15)	*650*	*2900*	*600*	*1100*	*1000*	*30*	*400*	*140*	*200*	*20*
La Campana§										
mean	340	8900	250	12300	1200	50	100	1200	120	40
SD	*120*	*4100*	*110*	*8000*	*700*	*20*	*40*	*600*	*70*	*20*
SE (n=16)	*70*	*2300*	*70*	*5300*	*400*	*20*	*20*	*400*	*40*	*10*
Nahuelbuta¶										
mean	70	8500	40	5400	1400	610	80	1300	110	70
SD	*20*	*1400*	*10*	*500*	*250*	*110*	*30*	*200*	*10*	*30*
SE (n=10)	*10*	*1000*	*10*	*300*	*180*	*80*	*20*	*100*	*10*	*20*

Standard deviation and standard error relate to the variability within the data set of each ecosystem. Where natural replicates were not available (i.e. in Pan de Azúcar), 10% relative uncertainty has been assumed.

† Pan de Azúcar ecosystem composition: 100% Nolona mollis; 32% and 68% relative leaf and stem growth, respectively, accounting for 5% leaf and 95% stem standing biomass

‡ Santa Gracia ecosystem composition: 25% each of Asterasia sp., Cordia decandra, Cumulopuntia sphaerica, Proustia cuneifolia; 32% and 68% relative leaf and stem growth assumed for all species, respectively, accounting for 5% leaf and 95% stem standing biomass

§ La Campana ecosystem composition: 5% each for Aristeguieta salvia and Colliguaja odorifera and 45% each for Cryptocaria alba and Lithraea caustica; 32% and 68% relative leaf and stem growth assumed for all species, respectively, accounting for 5% leaf and 95% stem standing biomass

¶ Nahuelbuta ecosystem composition: 60% Araucaria araucana, 10% Chusquea culeou, and 30% Nothofagus antarctica; 48% and 52% relative leaf and stem growth assumed for Araucaria araucana, respectively, accounting for 16% leaf and 84% stem standing biomass, 32% and 68% relative leaf and stem growth assumed for Chusquea culeou and Nothofagus antarctica, respectively, accounting for 5% leaf and 95% stem standing biomass.

https://doi.org/10.5194/bg-2020-69
Preprint. Discussion started: 9 March 2020

Table 6 Average $^{87}Sr/^{86}Sr$ ratio for bulk bedrock, bulk regolith, and the bio-available fraction in saprolite and soil. $^{87}Sr/^{86}Sr$ in bulk plants are weighted by the plant organs' relative growth rate and relative species abundance in the respective ecosystem (see Table 5). Radiogenic Sr composition for each single specimen are reported in Tables S2 (bulk regolith samples), S3 (bio-available fraction of saprolite and soil), and S5 (plant samples), respectively (Oeser and von Blanckenburg, 2020).

	bulk samples		bio-available samples		bulk living plants†	Seaspray input‡
	$^{87}Sr/^{86}Sr_{rock}$	$^{87}Sr/^{86}Sr_{regolith}$	$^{87}Sr/^{86}Sr_{sap}$	$^{87}Sr/^{86}Sr_{soil}$	$^{87}Sr/^{86}Sr_{plant}$	
Pan de Azúcar	0.7257	0.7305	0.7108	0.7099	0.7099	93%
SD	*0.0020*	*0.0036*	*0.0009*	*0.0007*		
Santa Gracia	0.7039	0.7044	0.7062	0.7062	0.7062	43%
SD	*0.0004*	*0.0003*	*0.0001*	*0.0001*	*0.0003*	
La Campana	0.7063	0.7053	0.7051	0.7053	0.7059	
SD	*0.0003*	*0.0002*	*0.0004*	*0.0005*	*0.0002*	
Nahuelbuta	0.7161	0.7162	0.7115	0.7111	0.7111	
SD	*0.0065*	*0.0036*	*0.0025*	*0.0023*	*0.0016*	
Seaspray*				0.7092		

* Seaspray composition from Pearce et al. (2015)

† Standard deviation corresponds to species-to-species differences in $^{87}Sr/^{86}Sr$

‡ Potential seaspray input into the bio-available fraction derived from a simple two-component mixing equation using bulk bedrock and seaspray as end-members. Substantial seaspray incorporation into the bio-available fraction in La Campana and Nahuelbuta is very unlikely (see text for discussion), therefore not shown.

Table 7 Nutrient recycling factors in Pan de Azúcar, Santa Gracia, La Campana, and Nahuelbuta. Shown in brackets are the Rec^X prior correction for atmospheric deposition.

	Rec^{Al}	Rec^{Ca}	Rec^{Fe}	Rec^{K}	Rec^{Mg}	Rec^{Mn}	Rec^{Na}	Rec^{P}	Rec^{Si}	Rec^{Sr}
Pan de Azúcar	1.1	1 (19)*	5.8	3 (3)*	30 (36)*	6	15 (16)*	4	0.26	3 (4)*
SD	*0.4*	*2*	*0.6*	*1*	*20*	*6*	*15*	*4*	*0.08*	*5*
Santa Gracia	0.1	1	0.4	6	1	1	1	5	0.04	1
SD	*0.5*	*4*	*0.5*	*3*	*3*	*3*	*1*	*13*	*0.07*	*3*
La Campana	0	2	0.1	2	1	0.5	0	9	0	1
SD	*0.1*	*2*	*0*	*5*	*1*	*0.6*	*0.1*	*15*	*0.01*	*2*
Nahuelbuta	0	6	0	15	3	190†	0.1	30	0.01	5
SD	*0*	*4*	*0*	*3*	*2*	*70*	*0.2*	*20*	*0.01*	*12*

* Rec^X in Pan de Azúcar has been corrected for atmospheric deposition of seaspray, ultimately decreases the recycling rates of weathering-derived nutrients by 95, 22, 18, 12, and 10% for Ca, K, Mg, Na, and Sr, respectively (see supporting information for further explanation and Fig. A6).

† values not being considered in the discussion as $W^{Mn}_{regolith}$ is potentially biased by high bedrock heterogeneities

https://doi.org/10.5194/bg-2020-69
Preprint. Discussion started: 9 March 2020

Biogeosciences Discussions Open Access EGU

Table 8 Turnover times for the soil and saprolite bio-available fraction with respect to the release by weathering and turnover times for bio-available fraction in soil with respect to uptake into plants.

study site	Al	Ca	Fe	K	Mg	Mn	Na	P	Si	Sr
						[yr]				
Pan de Azúcar										
$T^{X}_{bioav,\ soil,\ U}$	10	6040	0	490	280	40	910	710	480	1250
$T^{X}_{bioav,\ soil,\ W}$	10	n.d.	0	1590	10300	280	14800	2570	120	4670
$T^{X}_{bioav,\ sap.,\ W}$	40	n.d.	0	7570	27400	1240	20400	n.d.	490	10870
Santa Gracia										
$T^{X}_{bioav,\ soil,\ U}$	90	480	50	80	710	120	90	330	180	590
$T^{X}_{bioav,\ soil,\ W}$	10	600	30	510	730	230	60	1850	10	760
$T^{X}_{bioav,\ sap.,\ W}$	30	1150	80	300	2160	470	540	1760	30	1400
La Campana										
$T^{X}_{bioav,\ soil,\ U}$	780	530	660	50	460	1420	480	160	1970	820
$T^{X}_{bioav,\ soil,\ W}$	20	870	40	110	290	770	10	1470	3	530
$T^{X}_{bioav,\ sap.,\ W}$	20	1330	30	80	690	830	30	2050	10	950
Nahuelbuta										
$T^{X}_{bioav,\ soil,\ U}$	760	30	160	30	30	90	790	90	490	20
$T^{X}_{bioav,\ soil,\ W}$	20	170	10	400	70	17400	40	2900	10	120
$T^{X}_{bioav,\ sap.,\ W}$	0	150	0	190	80	4750	30	2130	10	210

$T^{X}_{bio-av.soil,U}$ = turnover time of element X in the soil bio-available fraction with respect to uptake into the ecosystem

$T^{X}_{bio-av.soil,W}$ = turnover time of element X in the soil bio-available fraction with respect to supply from dissolution of primary minerals and secondary precipitates

$T^{X}_{bio-av.sap,W}$ = turnover time of element X in the saprolite bio-available fraction with respect to supply from dissolution of primary minerals and secondary precipitates

n.d. = not determined; not determined turnover times because the respective inventory (Table 4) could not be determined